ION DENSITY MEASUREMENTS IN THE WAKE OF A HYPERSONIC SPHERE

L. Sevigny, et al

Defense Research Establishment

Prepared for:

Army Missile Command
Advanced Research Projects Agency

October 1972

DREV R-670/72
PROJ. 95-51-10

NON CLASSIFIÉ
UNCLASSIFIED

ION DENSITY MEASUREMENTS IN THE WAKE OF A HYPERSONIC SPHERE

L. Sevigny, D. Heckman and P. Caron

CENTRE DE RECHERCHES POUR LA DÉFENSE
DEFENCE RESEARCH ESTABLISHMENT
VALCARTIER

DEFENCE RESEARCH BOARD
CONSEIL DE RECHERCHES POUR LA DÉFENSE

Québec, Canada
October/octobre 1972

DREV R-670/72
PROJ. 95-51-10

NON CLASSIFIE
UNCLASSIFIED

ION DENSITY MEASUREMENTS IN THE WAKE OF A HYPERSONIC SPHERE

by

L. Sévigny, D. Heckman and P. Caron

This research was sponsored jointly by

The Defence Research Establishment
Valcartier
P.O. Box 880, Courcelette
Quebec, Canada

The Advanced Research Projects
Agency
ARPA Order 133
Monitored by the US Army
Missile Command
Redstone Arsenal
Alabama 35809
Contract DA-H01-69-C-0921

CENTRE DE RECHERCHES POUR LA DEFENSE
DEFENCE RESEARCH ESTABLISHMENT
VALCARTIER
Tel: (418) 844-4271

Québec, Canada

October/octobre 1972

RESUME

Dans ce rapport on tente de déterminer la valeur de la densité ionique au sein d'un sillage turbulent hypersonique produit par une sphère en titane de 2.7 pouces de diamètre, projetée à une vitesse approximative de 14,500 pi/sec dans un corridor de tir rempli d'azote. Deux pressions furent considérées, soit 7.6 torr et 20 torr. Le dispositif expérimental, la méthode d'enregistrement des signaux de sondes et leur échantillonnage ont été décrits dans un rapport précédent. Très succintement, le dispositif expérimental consiste en un double peigne transverse de sondes ioniques, la méthode d'enregistrement comprend une caméra Fastax 35 mm couplée à un oscilloscope et l'échantillonnage se fait au moyen d'un lecteur automatique commandé par un ordinateur.

Le courant capté par une sonde ionique de la dimension de celles employées au Centre de Recherches pour la Défense, Valcartier (CRDV) n'est pas directement proportionnel à la densité ionique locale et dépend même d'autres grandeurs physiques telles la température et la vitesse moyenne d'écoulement. Au cours des dernières années plusieurs interprétations théoriques du courant ionique ont été proposées. Elles peuvent être classées en deux catégories: les théories dites statiques, ne faisant pas intervenir la vitesse d'écoulement et les théories que nous qualifions de cinétiques où entre précisément la vitesse d'écoulement. Parmi les premières mentionnons les théories de Zakharova et al., Su et Kiel ainsi que celle de Schultz et Brown. En ce qui regarde les théories cinétiques il y a celle de Kulgein et les deux théories de Clements et Smy, l'une pour le cas d'une gaine mince et l'autre pour celui d'une gaine épaisse. Comme on le voit le menu est varié. Aussi, plutôt que de sélectionner une théorie a priori, nous les avons toutes programmées de façon à pouvoir par la suite confronter les résultats fournis par chacune d'elles.

Divers laboratoires ont établi expérimentalement que la forme des profils radiaux de la densité ionique, ou électronique, était assimilable à une courbe d'expression générale suivante: $A \exp-(R/B)$, soit une

gaussienne. Par conséquent, une fois la densité ionique calculée, la méthode d'analyse procède comme suit: les mesures appartenant à l'une ou l'autre des deux pressions utilisées sont d'abord groupées dans des bandes axiales délimitées de la façon qui s'avère la plus avantageuse tant du point de vue de la résolution que de celui de la précision statistique. Les profils radiaux ainsi définis sont par la suite lissés individuellement par une fonction gaussienne selon la méthode des moindres carrés. Les deux paramètres déterminés sont: la valeur de la densité ionique le long de l'axe de vol, et la largeur du sillage ionique. Les résultats obtenus sont comparés avec ceux relatifs à la densité électronique provenant de mesures à l'aide d'un interféromètre micro-onde et de sondes de Langmuir.

Il ressort des faits présentés dans ce rapport que les prédictions des théories statiques concernant la valeur de la densité ionique le long de l'axe de vol sont pratiquement un ordre de grandeur plus élevées que celles des théories cinétiques, à 7.6 torr comme à 20 torr. Par ailleurs, la valeur de la densité ionique prédite par les théories cinétiques est plus grande que la valeur de la densité électronique mesurée avec l'interféromètre. Plus explicitement, à 7.6 torr il semble que la valeur prédite par les théories cinétiques soit un facteur 5 trop élevée autour de 100 diamètres derrière le projectile; toutefois, plus loin dans le sillage (240 - 400 diamètres), les sondes ioniques, l'interféromètre et les sondes de Langmuir donnent les mêmes résultats en dedans d'un facteur 2. Par contre, à plus haute pression (20 torr) l'écart entre les valeurs des sondes ioniques et de l'interféromètre micro-onde s'accroît et atteint presque un ordre de grandeur. Ces constatations semblent signifier que 'La Théorie' des sondes ioniques est loin d'avoir vu le jour. Néanmoins, toutes les théories s'accordent sur un point: la densité ionique le long de l'axe de symétrie du sillage décroît selon une loi de la forme:

$$n_o \propto (X/D)^{-2}.$$

En plus des résultats se rapportant à la valeur de la densité ionique sur l'axe, ce rapport fournit des données intéressantes sur la largeur du sillage ionique. Il contient également beaucoup de renseignements sur le dépouillement et le traitement des signaux de sondes de même que sur les diverses théories des sondes ioniques. Quant aux appendices, ils renferment des tableaux où se trouvent rassemblées des données relatives aux lissages des profils radiaux pour toutes les théories étudiées, et une série de figures montrant l'évolution des profils radiaux de la densité ionique en fonction de la distance au projectile.

ABSTRACT

A report is presented of the results of a major research effort undertaken to determine experimentally, through the use of cylindrical electrostatic probes and existing probe theory, the levels of ion density in the turbulent wakes behind 2.7 inch diameter spheres flown at 14,500 feet/second in a ballistic range filled with nitrogen at 7.6 torr and at 20 torr. The major problem encountered in this work is the one concerned with the theoretical interpretation of the ion current seen by an electrostatic probe in terms of ion density. The many theories which have been proposed can be divided into two main categories: the 'static' theories which do not consider the flow velocity of the plasma in which a probe is immersed and the 'kinetic' theories which attempt to take flow velocity into account. Generally speaking, the theories indicate that the current collected by an ion probe of convenient dimensions is not uniquely determined by the ion density, but also depends on such physical variables as the temperature, pressure, probe potential, and additionally, in the case of the 'kinetic' theories, on the bulk velocity of the medium. Where the 'problem' arises is in the fact that the probe theories differ in their predictions of the details of the dependence of the probe current on the various physical variables listed above.

Measurements of the ion current distribution across hypersonic sphere wakes have been made by means of a transverse survey array of cylindrical electrostatic ion probes. Three static theories and three kinetic theories have been applied to the mean current data of the probes, and with the aid of experimentally measured temperature and velocity distribution data for sphere wakes, used to construct radial distributions of ion density estimates for each theory. These radial distributions have been fitted with gaussian curves by the method of least mean squares. Two parameters of the ion density distributions are determined: the ion density on the axis of the wake and the ion density radius of the wake. These results have been compared with electron density levels in the wake deduced from microwave interferometer measurements and Langmuir probe instrumentation.

Concerning the ion density level on the wake axis, it is found that the static theories predict ionization levels which are an order of magnitude larger than those given by the kinetic theories at both 7.6 and 20 torr. In turn, the kinetic theories predict ion density levels which are higher than the electron density levels obtained with the interferometer. At 7.6 torr, the kinetic theories seem to be about a factor of five too high at 100 diameters behind the sphere, but at larger axial distances, (240 - 400 diameters) the ion density results of the ion probes, and the electron density results of the interferometer as well as the results of the Langmuir probe, are all within a factor of 2. However, at higher pressures (20 torr) the difference in the results increases and the kinetic theory ionization levels are about an order of magnitude higher than the microwave interferometer results. One of the conclusions from these results is that 'The Theory' of cylindrical electrostatic probes has yet to see the light of day. The predictions of all the diverse theories agree on one point: between the axial distances of 100 and 400 diameters, the ion density on the wake axis decays according to an $n_o \propto (X/D)^{-2}$ law. In addition to the results concerning ion density levels, interesting information has also been generated concerning the widths of the ion density profiles in the wake.

The report includes considerable information on the treatment of the probe current signals and on electrostatic probe theories, while Appendices include tables of data pertaining to the fitting of the ion density radial distributions derived from each of the theories, and graphs showing the evolution of the ion density radial distributions with axial distance behind the projectile.

TABLE OF CONTENTS

1.0 INTRODUCTION

During the past five years, considerable progress has been made in measuring the behavior of various physical quantities in the wakes of hypersonic spheres. The present report is concerned with the experimental determination with electrostatic probes of the ion density levels in the turbulent wakes of 2.7 inch diameter titanium spheres flown at 14,500 feet/second in a ballistic range filled with nitrogen at pressures of 7.6 and 20 torr. Through the use of a transverse array of ion probes inserted across the wake, measurements have been made of the radial distribution of the saturated ion currents collected by the probes. These probe currents (or their voltage equivalents) have been recorded on 35 millimeter film with oscilloscopes and Fastax cameras, the resulting analog signals digitalized by a computer-driven film reader, and the digital data processed on a large XDS computer. A detailed description of many of these techniques has recently been published (Reference 1). The further exploitation of the current data to derive the characteristics of the charge density in the wake will be described below.

The current collected by an ion probe of the dimensions of those employed at The Defence Research Establishment Valcartier (DREV) is not directly proportional to the local ion density, but because of continuum flow effects, depends on other physical quantities such as the temperature, pressure, and the mean flow velocity. In the course of recent years many theoretical interpretations of the ion current drawn by a cylindrical probe have been proposed. These can be classified into two categories: The 'static' theories which neglect the effect of the flow velocity of the medium relative to the probe and the 'kinetic' theories which attempt to account for flow velocity effects. In the first category fall the theories of Zakharova et al. (Reference 2), Su and Kiel (Reference 3), and Schulz and Brown (Reference 4). Among the kinetic theories is that due to Kulgein (Reference 5) and the two due to Clements and Smy, one for the case of a thin sheath (Reference 6) and one for the case of a thick sheath (Reference 7). Obviously, the choice

of theories is rather large. Rather than select one or two theories on an a priori basis, we have chosen to employ all six of the above mentionned theories to estimate the ion density in the wake. The various results can then be compared among themselves as well as with the results obtained by other techniques.

It has been observed at several laboratories (References 8 - 10) that the experimentally obtained distributions of ion density or electron density in wakes and in jets are amenable to being fitted by the gaussian expression $A \exp(-(R/B)^2)$. At DREV, the gaussian distribution has been extensively employed to fit radial distributions of wake velocity estimates at various axial distances behind the projectile (Reference 1). The stages in the curve-fitting procedures such as the definition of the axial bands, the manner of obtaining the fit, the computation of the intervals of confidence, etc., have been described in detail in a previous report (Reference 1). Once the estimates of ion density for a given theory have been obtained from the probe currents averaged from 0.5 millisecond segments of the probe signals, then exactly the same procedures as were used in the case of velocity can be applied to the calculation of the particular ion density distribution for that theory.

In a previous DREV report on the use of cylindrical electrostatic probes, Cantin (Reference 11) has assembled considerable information relative to the plasma properties of the wake and has treated in detail the three static theories previously mentioned as well as the kinetic theory of Kulgein. By expressing the functional dependence of the probe current on the dependent variables in a power law form, Cantin was able to estimate the effect on the mean current of the auto-and cross-correlation coefficients of various combinations of variables when the probe was immersed in a turbulent wake. As part of the analysis, preliminary data from two early trials in air atmospheres at 20 and 76 torr were examined. It was concluded that the mean current could be calculated by inserting the mean values of the variable into the theory to an accuracy of 10 to 20% depending on which of the four theories

considered in the report was applied. Finally several appendices in the report were concerned with the description of APL language programs for the calculation of ion densities from experimental measurements.

The present document, in fact, is in logical succession to the report by Cantin on the use of ion probes for wake diagnostics (Reference 11). Cantin was mainly concerned with examining the implications of particular probe theories as regards the interpretation of the mean and fluctuating components of the ion currents in terms of the mean and fluctuating ion densities in the wake. In the present investigations, we apply the various probe theories to a large number of experimental measurements of probe current with the twin objectives of finding at least one accurate theory and of inferring the characteristics of the mean ion density distributions in the wake. In order to realize more favorable conditions, the measurements have been taken in nitrogen atmospheres, because only positive ions (N_2^+ and N^+) should be present in nitrogen wakes, and because of the availability of experimental temperature distribution data for this case. Certain advances have also been made in the programs used to analyze the current measurements. APL becomes inappropriate when the amount of data to be handled becomes very large; consequently all the old programs and the new programs have been done in FORTRAN.

2.0 EXPERIMENTAL TECHNIQUE AND DATA RPOCESSING

The transverse array of ion probes used to survey ionization in the wake is seen in one of its forms in Figure 1. The basic element of such an array consists of two cylindrical probes imbedded at a fixed separation in a thin support about 12 inches high. Both collecting wires are normal to the mean flow direction of the wake, and are mounted so that a line parallel to the wake axis passes from a point on one probe through the corresponding point on the other (Figure 2). Eight such elements set in a transverse configuration, with a lateral spacing of

1.25 inches between adjacent elements, give the array its capability to survey the wake. The current collected by the negatively biased central electrode of each probe is transmitted directly to one of the 16 current-to-voltage preamplifiers located in the wedge-shaped housing above the array (Figure 1). These preamplifiers supply bias to the probes and also drive the ten to twelve feet of cable required to lead the signal to the exterior of the flight chamber of the range. The signals are then passed through power amplifiers and transmitted on long 92 ohm cables to the recording room, where they are displayed on oscilloscopes and photographed on 35 millimeter film. A more detailed description of the characteristics of the probes, the array, and the recording system has been published (Reference 1).

2.1 Sampling of the Analog Signal Traces

The two signals from the pair of probes in any one of the basic two-probe elements of the transverse survey array are recorded simultaneously on the same roll of 35 millimeter film. Thus the raw results of any trial with the survey array consist of a dozen or more rolls of film, each streaked by two wiggling black lines representing probe signals. The first step but one in the data reduction process is the sampling of these signal traces. Before this can be done, a positive must be made, in order to convert the recorded signal into a transparent trace on an opaque field. This positive can then be processed in the DREV automatic film reader. In the reader, the image of a luminous spot from the screen of a precision cathode ray tube is projected on the film. An optical system behind the film receives the transmitted light and focusses it on a photomultiplier. Simultaneously, a fraction of the light emanating from the spot is diverted by a beam splitter, and after transmission through an optical system similar to the first, is sent through a uniform density filter onto a second photomultiplier. The comparison of the ouput signals of the two photomultipliers reveals if the region illuminated on the film is opaque or transparent. The result of this comparison in entered into a digital computer capable of registering the coordinates of the spot.

Both signal traces recorded on the film are sampled simultaneously at the same sampling frequency. In the reading process, the luminous spot appearing on the cathode ray face is swept from bottom to top and from left to right. When the beam arrives at the upper right corner of the screen, the film is automatically advanced, and the scanning beam returned to the lower left hand corner of the screen in order to recommence the scanning. The length of the film swept in one scan is about 0.5 inch. Normally if the apparatus was in perfect adjustment, the point where the swept beam picked up the signal on the first upward sweep would correspond exactly to the point seen by the beam on the last sweep of the previous scan. The coordinates of the signal in the last reading of one scan and the first reading of the next scan must be contiguous. The adjustment of the reader is rarely perfect, so that, in practice the two readings may differ. Should the readings differ, the computer section of the reader will effectively raise or lower the zero reference of the signal in order to be able to continue sampling the signals without introducing a fictional step discontinuity in the output. This adjustment takes place after each advance of the film.

Obviously, if such an internal operation of the film reader could not be taken into account, it would render impossible the task of attempting to measure accurately the absolute level of the recorded signals, particularly at low signal amplitudes. When one states that the reader raises or lowers the reference level, this is only a way of describing the result of an internal operation of the machine. In actual fact the reading expressing the ordinate of a point on one of the two signal traces on the film is always measured from an imaginary line which joins the top of the perforations which allow the driving of the film. The correction which the reader attaches to this reference line after the film is advanced is printed out on the teletype machine which is part of the input-output equipment of the reader. This correction can be different for the two signal traces.

Table I supplies an example of the communications between the operator and the data reader during the reading of a film. The column of numbers immediately below the words 'CAL DATA' are furnished by the operator. They identify the film which he is preparing to read. The four column matrix located a little below is printed out by the reader. Each line corresponds to one advance of the film. The first and second numbers in a line represent the gap between the ordinates of the first and last points of two successive section of film, for the lower trace and the uppper trace respectively. The last two numbers give the accumulative or total displacement of the reference level since the beginning of reading for each of the signals. For example, consider the last element in the last line of Table I, i.e. 20. This element indicates that the readings of the upper trace of the corresponding segment of signal are all high by 20 units. Consequently, when the time arrives to calculate the mean signal level it will be necessary to take account of this error introduced in the average level by the operation of the film reader.

The numerical values corresponding to the sampled points of the probe signals are inscribed on a magnetic tape by the data reader. In the next step, this tape is read and decoded by the XDS Sigma 7 computer facility at DREV. At the same time, the computer controlled printer reproduces a graphical representation of the sampled signal. The following step in the data handling consists of the preparation of input data necessary for the correlation and averaging of the digital traces. (In the following pages we will use the expression 'digital trace' in preference to the term 'sampled signals').

2.2 Correlation of the Digital Traces

The manner in which are correlated the digital traces of the signals from a pair of probes is illustrated in Figure 3. The graph in the upper left corner represents a segment of the digital traces resulting from the sampling of the signal on 35 millimeter film. The upper signal, which is from the upstream probe in a pair, is divided into segments of

0.5 millisecond in length (Reference 1). Each of these segments is then cross-correlated with a segment taken from the downstream probe (or lower signal). The length of the cross-correlation so calculated depends on the distance separating the probes and on the local velocity in the wake. Mathematically, the process can be expressed by

$$R_j = \frac{\sum_{i=1}^{N} (x_i - \bar{x})(y_{i+j} - (\bar{y})_j)}{\sqrt{\overline{x^2}}\ \sqrt{(\overline{y^2})_j}} \quad , \ j = 0,1,2,\ldots r \tag{1}$$

where $\bar{x} = \frac{1}{N} \sum_{i=1}^{N} x_j$; $(\bar{y})_j = \frac{1}{N} \sum_{i=1}^{N} y_{i+j}$

$$\sqrt{\overline{x^2}} = \frac{1}{N-1} \sum_{i=1}^{N} (x_i - \bar{x})^2,$$

$$\sqrt{\overline{y^2}} = \frac{1}{N-1} \sum_{i=1}^{N} (y_{i+j} - (\bar{y})_j)^2.$$

In these expressions x_i represents the digital trace of the upstream probe and y_i that of the downstream probe. Since the determination of the cross-correlations for velocity estimation (Reference 1) necessitated the calculation of the mean values and the root mean square values of the digital traces, and since all these data have previously been stored on magnetic tapes, all the information required to evaluate the mean current drawn by the various probes is readily available.

We will now give some explanation of the manner in which information concerning the cross-correlation coefficients is stored on magnetic tape. As previously mentionned, a cross-correlation is calculated for each 0.5 millisecond segment of the digital trace. To each one of these segments is allocated an 'analysis number'; the actual number is determined by the point on the film at which it is decided to begin

analyzing. Thus to any segment, there corresponds an analysis number and a vector R formed form r + 1 elements representing the calculated values of the cross-correlation coefficient R_j. This vector defines on the magnetic tape a physical record structured in the following way

$$(r+1), (R(I), I=1, (r+1)),$$

which is to say that the number of elements in the vector appears at the head of the listing. Furthermore, this record is always preceded by another record containing exactly 20 elements. This last record is required because of the necessity to identify the vector R by giving the number of the round (trial) to which R belongs, the number of the camera on which were recorded the corresponding pair of signals, the gain of the oscilloscopes, the analysis number, etc. Moreover, the five last memory elements contain respectively the value of R_j for $j = 0$ (i.e. the value of the space correlation coefficient for the two probes involved), the mean value $(\bar{x})$ and the root mean square fluctuation $(\sqrt{\overline{x^2}})$ of the digital trace of the upstream probe, and finally the values of $(\bar{y})_j$ and $(\sqrt{\overline{y^2}})_j$ for $j = 0$ for the downstream probe. For a more complete description of this vector we can return to Table II. In the various computer programs it is customarily given the name CAL. In order to be in a position to distinguish the identification code record from the one containing the vector R, the negative number minus 20 is alwasy written at the beginning. This has equally the effect of structuring the two records in the same manner. The method of storing the results of the cross-correlation computation of any given round on magnetic tape thus consists of alternating, without interruption, from one end of the tape to the other, the two records described above. All the analyses belonging to the same round are placed one after another in any order. If for one reason or another, it is necessary to recompute one or more analyses, the retakes are inscribed at the end of the analyses previously computed, with the precaution of adding a decimal after the analysis number to permit its differentiation from the previous calculation, when so desired.

3.0 DETERMINATION OF MEAN CURRENT COLLECTED BY A PROBE

In the preceding section we have seen that the current signal detected by a probe immersed in an ionized turbulent wake undergoes many transformations before finally ending in the form of a digital trace susceptible to further manipulation on a digital computer. We can express the transfer function between the probe signal and its digital trace as follows:

$$I = \frac{(A_o - A) \cdot G}{R_F \cdot G_{AL} \cdot G_L \cdot F}, \qquad (2)$$

where

- R_F is the feedback resistor of the current to voltage preamplifier (0.2 Megohms)
- G_{AL} is the gain of the linedriver amplifier
- G_L is the magnification factor between the screen of the oscilloscope and the 35 millimeter film in the Fastax camera (0.35)
- F is the vertical scale factor (or frequency) in the PDP-5 automatic film reader (758 counts/centimeter)
- G is the sensitivity employed on the oscilloscope
- A_o is the zero reference level of the digital trace
- A is the value (in counts) of any point of the digital trace

and

- I is the current collected by the probe.

The quantities R_F, G_L, and F described above are universal constants, in the sense that they have the same value for all recent rounds. Consequently, if in equation 2 we replace them by their numerical values we obtain

$$I = 18.846 \left[\frac{(A_o - A) \cdot G}{G_{AL}}\right] \qquad (3)$$

where

I is now expressed in nanoamperes,

G is in volts/centimeter

and

A is in counts.

Equation 3 has been used to determined the mean current detected by a probe. The values of G and of G_{AL} are determined at the time of the trial. If it is desired to calculate the mean current of the upstream probe, A is equated to $\bar{x}$, or if it is desired to calculare the mean current to the downstream probe, A is equated to $(\bar{y})_o$. In either case, the required information can be found written on magnetic tape as has been described in detail in the preceding section. The only thing still lacking for the calculation of the mean current to any specific probe is the true zero level of the digital trace, or A_o. In the first approximation, A_o is determined by averaging two arithmetic means. The first of these means is obtained by averaging over a segment of signal recorded just before the passage of the projectile (i.e. before the probe begins drawing current) and the second mean is obtained from a segment of signal corresponding to the far wake where it is reasonable to assume that the probe no longer draws any current. However, there are two sources of error which can affect the zero level as found by this procedure. The first consists of errors introduced by the film reader during the sampling of the analog traces, particularly when compensating for film advance. The second, less evident but more easily understood, results from the lack of absolute precision in the drive mechanisms of the apparatus which are used for contact printing of the Fastax camera film to obtain a positive for the data reader. We will return to this problem in the following paragraphs. For the moment, let us note simply that whenever possible, the zero level has been adjusted in such a way as to minimize the effect of these errors. When it proved difficult to evaluate one or the other of these errors (or both), the actual zero level was estimated by reading it directly from the 35 millimeter film with the aid of a calibrated ocular. Once the value of the zero level, A_o, is determined, one can proceed using equation 3 to calculate the gross mean current (i.e. the non-corrected mean current) for the probe being considered.

Let us now consider in more detail the errors affecting the zero reference level. The first of the errors mentioned above, that introduced by the reader during the sampling of the analog signals, has been described in the preceding section. It was seen that the reader raised or lowered the reference level after each advance of the film, although the teletype furnished an accounting of these changes (Table I). Thus available is a list of corrections similar to that in Table I for each pair of analog signals which has been digitalized by the reader. Given such a list it is neither possible nor necessary to correct individually every point of a digital trace. A global correction applied to the mean value $\bar{x}$ or $(\bar{y})_o$, previously defined, is perfectly adequate. To carry out the correction process automatically, it is necessary to establish a correspondence between the analysis numbers and the list of corrections for a pair of signals. Now one knows from observation that the reader samples a total of about 512 points before advancing the film and subsequently it reads an average of 269 points before each subsequent advance. Thus the sampled points are numbered consecutively according to the chronological order of reading, the first line of the matrix of Table I refers to all the points of which the number (or the address) is included between 512 and 781 (512+269); the second line refers to those between 781 and 1050 and so forth. In this manner one arrives at the construction of Table III. The procedure which permits the extraction from this table of the appropriate correction to the zero reference level for a particular analysis number is straightforward. As one can see from Table II, the code which identifies the cross-correlation coefficient of any 0.5 millisecond segment of signal from an upstream probe with the corresponding segment of a downstream probe contains not only the number of the round, the analysis number, etc., but also the address of the first and last points of the upstream probe signal. Given this last information it is sufficient to look into Table II to discover which line of Table I contains the correction for the analysis number under consideration. This can be accomplished very quickly by juxtapositioning Tables I and III. In the next step, a computer program calculates the current equivalent of the zero level correction from Table I by the use of equation 3. This

correction is added to or subtracted from the gross mean current calculated previously. The final results of these corrections are stored on magnetic tape pending the following step which consists of the final restoration or correction of the mean probe currents.

We now turn to the second source of error affecting the zero reference level of the digital signals. In order that the film reader can sample a signal recorded on 35 millimeter film, the latter must appear as a transparent line on an entirely opaque background. Therefore it is necessary to take the original film negative and make a positive for reading purposes. The positive is made by contact printing on another strip of 35 millimeter film. In a perfect world, the positive thus obtained would complement exactly the original negative. However, because of the slack in the driving mechanisms of the printer and the clearances necessary so that the teeth on the driving sprockets may turn smoothly in the perforation on the sides of the film, it happens frequently during the printing operation that the two films become offset with respect to one another. In this case perforations of the original film (negative) do not coincide exactly with those of the positive, and one can thus observe a shadow around the perforations in the positive. Fortunately, these shadows permit a measure of the displacement of the two films and thus provide a simple means to quantify the effect on the reference level. In fact, any relative displacement of the two films results in an alteration of the reference level of the positive. Instead of being a straight line, the reference level on the positive becomes a more or less undulating line. Consequently we must make an additional correction to the gross mean current. To estimate this correction, we begin by measuring the displacement at every fifth analysis. If the observed maximum displacement is less than 0.05 millimeter (4 counts), or if it is possible to reduce the error to this value by modifying the zero level of the signals, no correction is made for this source of error. In the opposite case, the correction for positive-negative displacement is integrated with the film reader-induced error previously described so as to obtain a single correction. A computer program will then correct both errors at the same time.

The current drawn by an electrostatic probe immersed in a hypersonic turbulent wake decreases rapidly as the projectile recedes from the probe or vice versa. This is so much the case that it is necessary to record the probe signals at several different gains if one wishes to make measurements from just behind the projectile to several hundreds of diameters of axial distance in the wake. Given the same signal recorded at one or more gains with obviously some overlapping, it consequently becomes indispensable to undertake a certain amount of editing when attempting to determine a consistent history of the mean current collected by a given probe. In the first phase, one has to define the useful portion of each recording of the same probe current, by defining the analysis number at the beginning and at the end of the portion. The first of these is obtained simply by visual inspection of the signal to determine where the readable part of the signal begins. To determine the second, we are led to consider a threshold for the signal level corresponding more or less to the level of the noise. Such a consideration carries with it a certain amount of arbitrariness. Nevertheless, there is little risk in deciding that there is nothing to be gained in conserving mean current values when the relative error exceeds 100 percent. Consequently, it has been decided to take as a threshold for all the points of a digital trace the value of the mean current which corresponds to an imprecision of ± 15 counts. These limits include ± 4 counts to take account of the slow oscillation which always seems to be present in the segments of the trace (before and after) which are used to determine the zero signal level; ± 2 counts because the correction of the error introduced by the data reader applies to the mean value of the points of a 0.5 millisecond segment and not to the points themselves; ± 4 counts for the residual displacement of the negative and positive due to the printing process; and finally ± 5 counts representing the mean width of the analog signal. On this basis, the threshold of any signal corresponds to the value of current given by

$$18.846 \times 15 \times G/G_{AL}.$$

Once the useful sections of all the recordings of the signal from a given probe have been defined in accordance with these procedures, the information is supplied to a computer program. This program makes the final selection of the segments of probe signal, keeping, for each analysis number, only the mean current which was recorded by the oscilloscope having the highest sensitivity.

The calibration of all apparatus employed in the recording of the probe signals was periodically verified. In this fashion it was possible to assure the proper functioning of the preamplifiers associated with the probes. In addition, the effects of the 170 feet of cable in the transmission line between the line driver amplifiers and the oscilloscopes in the recording room were also periodically checked; the method involved sending a signal of known amplitude and of a frequency of 1.0 kilohertz through the system and measuring the resulting deflection on the cathode ray tube of the oscilloscope. The transmission factor of the line-driver-amplifier-terminated-line system was about 0.9. Correction for these transmission losses provides a final adjustment that must be made to the mean currents detected by the probes.

4.0 MATHEMATICAL FORMULATION OF VARIOUS THEORIES OF ION COLLECTION BY CYLINDRICAL PROBES

For the interpretation of cylindrical electrostatic probe measurements in hypersonic turbulent wakes under the conditions usually encountered in ballistic ranges, the basic collisionless theory of Langmuir becomes completely inapplicable, because the probes are immersed in a collision-dominated flow (Reference 1). In the course of the years, many alternative theories for cylindrical probes in continuum flow have been proposed; however, it seems quite possible that 'The Theory' of electrostatic probes has not yet seen the light of day. In this situation, we have simply decided to program all of the available theories and to see to what sort of predictions they lead.

The objective of this section of the report is to give résumés of the mathematical formulations into which the various theories have been manipulated for the purposes of computation of ion densities in the hypersonic turbulent wake. For further details on a number of the probe theories, the reader is referred to the report by Cantin (Reference 11).

4.1 Definition of Some Physical Quantities

4.1.1 Current Density

If I is the current collected by a cylindrical probe of length ℓ and radius a, then by definition, the current density at the surface of the probe is given by

$$J = I/2\pi\ell a.$$

If J is expressed in milliamperes/cm^2, I in nanoamperes, and a and ℓ in millimeters, then one obtains

$$J = 1.591 \times 10^{-5}\ I/\ell a. \qquad (4)$$

4.1.2 Ion Mobility

After the first approximation of the Chapman-Enskog theory, the mobility of ions can be written (Reference 12) as

$$\mu_i = \frac{3\sqrt{\pi}\ e}{8N(2kTM_R)^{\frac{1}{2}}\sigma} \qquad (5)$$

where
- μ_i is the ion mobility
- e is the electron charge
- N is the neutral particle density
- k is the Boltzman constant
- T is the temperature

M_R is the reduced mass

σ is the collision cross-section.

The reduced mass M_R is defined by

$$M_R = mM/(m+M)$$

where M represents the ion mass and m the mass of a gas molecule.

From the kinetic theory of gases it is shown that

$$\sigma = 1/\sqrt{2}\,\lambda_i N$$

where λ_i is the mean free path for ions. The mobility at any pressure and temperature can be written in terms of the mobility μ_o at 760 torr and 273° K by an equation of the form (Reference 11)

$$\mu_i(p,T) = \mu_o \left(\frac{760}{p}\right) \sqrt{\frac{T}{273}}. \qquad (6)$$

The pressure p is measured in torr; μ_o was taken equal to 1.7 cm^2/Volt-sec.

4.1.3 Ion Mean Free Path

From equations 5 and 6 it follows that

$$\lambda_i = 1.426 \times 10^{-8}\, \mu_i \sqrt{TP_R} \qquad (7)$$

where λ_i is measured in centimeters and μ_i is measured in cm^2/volt-second. The quantity P_R is equal to the product of the reduced mass with Avogadro's number.

4.2 Static Theories

4.2.1 Theory of Zakharova

From equation 4b in the paper by Zakharova et al. (Reference 2), we can show that

$$n_i = \left[\frac{4}{0.85e}\sqrt{\frac{\pi}{8kN_A}}\right]\left(\frac{a}{\lambda_i}\right)\frac{\sqrt{P_M T}}{T_e} J_i \ln\left(\frac{\ell}{ax_o}\right) \qquad (8)$$

where n_i is the ion density

N_A is Avogadro's number

P_M is the molecular weight of the ion

T_e is the electron temperature

$x_o = (1 + u)(1 + \alpha u)$

$$u = \frac{2.3 \times 10^{-2}}{a}\left(V^3\lambda_i / J_i^2 P_M\right)^{1/5}$$

$\alpha = 0.5$ for cylindrical probes

and V is the voltage on the probe.

Other symbols have previously been defined.

If the various constants in equation 8 are replaced by their numerical values we obtain

$$n_i(\text{cm}^{-3}) \times 10^{-10} = \frac{20.25\ a(\text{mm})\ J_i(\text{mA/cm}^2)}{\lambda_i(\text{cm})\ T_e(^\circ\text{K})}\sqrt{P_M T}\ \ln\left(\frac{\ell}{ax_o}\right). \qquad (9)$$

It is assumed here that $T_e = T_i = T$.

4.2.2 Theory of Su and Kiel

Equation 2.3 of the article of Su and Kiel (Reference 3)

$$I_i = n_i \left[2\pi\ \ell\ k(T_e + T_i)\mu_i / \ln(\pi\ell/4a)\right] \qquad (10)$$

contains only symbols which have previously been defined. Replacing the constants by their numerical values we obtain

$$n_i(cm^{-3}) \times 10^{-10} = \frac{a(mm)J_i(mA/cm^2)}{\mu_i(cm^2/Volt\text{-}sec)} \left[\frac{\ell n\ 0.7853\ell/a}{1.38076\ (T_e+T_i)}\right] x10^9. \quad (11)$$

4.2.3 Theory of Schulz and Brown

The equations derived by Schulz and Brown (Reference 4) are

$$I_i = 2\pi\mu_i\varepsilon_o V^2 a^{-2}\gamma^2 \quad (12)$$

$$I_i = 2\pi a\ell J_r(r_g/a)\ (3/2\ \alpha p) \quad (13)$$

$$\gamma = \left[(r_g/a)^2-1\right]^{\frac{1}{2}} - (r_g/a)\ \ell n\ \{r_g/a+\left[(r_g/a)^2-1\right]^{\frac{1}{2}}\} \quad (14)$$

$$J_r = en_i(kT_i/2\pi M)^{\frac{1}{2}} \quad (15)$$

where

ε_o is the permittivity of free space

and

r_g is the radius of the sheath.

The value of the constant α appearing in equation 13 was determined empirically by Schulz and Brown. However, Kulgein (Reference 5) has shown that

$$\alpha = \left[9/8\lambda_i p(1 + T_e/T_i)\right] a\ \ell n(\ell/a). \quad (16)$$

(It should be noted that there is no relation between the α defined in equation 16 and that defined in the theory of Zakharova)

To simplify the solution of the set of equations (12 - 15), it is convenient to find the inverse of equation 14, so that the normalized sheath radius r_g/a is expressed as a function of γ. The solution given by Cantin (Reference 11) is

$$r_g/a = \exp\left[A(\ell n\gamma)^2 + B\ell n\gamma + C\right] \qquad (17)$$

where $A = 0.0451$

$B = 0.3663$

and $C = 0.7717$.

In solving the equations, γ is first obtained from equation 12. Then r_g/a is found from equation 17. Substituting equation 15 into equation 13 and replacing the constants by their values, one obtains finally the ion density

$$n_i(cm^{-3}) \times 10^{-10} = \frac{1.1478 J_i (mA/cm^2)\sqrt{P_M/T_i}\,x10^2}{(r_g/a)(1/\alpha\, p)} . \qquad (18)$$

4.3 Kinetic Theories

4.3.1 Theory of Kulgein

Kulgein (Reference 5) employs the same equations as Schulz and Brown but he assumes that because of the flow velocity, only the forward half of the surface of the cylindrical probe collects ions. Thus equation 12 is replaced by

$$I_i = \pi\mu_i\varepsilon_o\ell V^2 a^{-2}\gamma^{-2}. \qquad (19)$$

The factor γ which depends on the sheath radius r_g/a can be evalued as previously. In addition Kulgein obtains

$$I_i = 2en_i\ell U(1-a^2/r_g^2)a, \qquad (20)$$

where U is the local flow velocity.

From these equations, one can show that the ion density is given by

$$n_i(cm^{-3}) \times 10^{-10} = \frac{6.44 \times 10^4 \times J_i\ (mA/cm^2)}{U(ft/sec)\ (a/r_g - r_g/a)} . \qquad (21)$$

4.3.2 Thin Sheath Theory of Clements and Smy

The theory of Clements and Smy (Reference 6) for the case of a cylindrical probe surrounded by a thin sheath leads to the following relation between the probe current I_i and the ion density n_i

$$I_i = 5.3\ (\varepsilon_o \mu_i a)^{\frac{1}{4}} (eUn_i)^{\frac{3}{4}} V^{\frac{1}{2}} \ell . \qquad (22)$$

Replacing the constants by their numerical values, rearranging terms and changing the system of units, we obtain

$$n_i(cm^{-3}) \times 10^{-10} = 5.774 \times 10^6 \left[\frac{J_i^4(mA/cm^2)}{\mu_i(cm^2/Volt\text{-}sec)V^2(Volt)}\right]^{1/3} \frac{a(mm)}{U(ft/sec)} . \qquad (25)$$

4.3.3 Thick Sheath Theory of Clements and Smy

Clements and Smy (Reference 7) have published a second theory treating the case where the probe is surrounded by a thick sheath, and leading to the relation

$$I_i = \frac{2(\pi \mu_i \varepsilon_o)^{1/3} (n_i eUV)^{2/3} \ell}{[\ell n(I_i/2n_i eUa\ell)]^{2/3}} . \qquad (24)$$

This equation can also be written as

$$\left(\frac{\pi J_i}{eUn_i}\right) \ell n \left(\frac{\pi J_i}{eUn_i}\right) = \frac{V}{a} \sqrt{\frac{\mu_i \varepsilon_o}{a\ J_i}} . \qquad (25)$$

By normalizing n_i by 10^{10}, it can be shown that

$$\frac{\pi J_i}{eUn_i} = 6.442 \times 10^{4} \left(\frac{J_i(mA/cm^2)}{U(ft/sec)n_i(cm^{-3})}\right)$$

and

$$\frac{V}{a}\sqrt{\frac{\mu_i \varepsilon_o}{a\ J_i}} = 2.975 \times 10^{-4}\left(\frac{V(volt)}{a\ (mm)}\right)\sqrt{\frac{\mu_i(cm^2/Volt\text{-}sec)}{a(mm)J_i(mA/cm^2)}}$$

A computer subroutine is used to numerically invert equation 25 to obtain n_i.

5.0 ANALYTICAL EXPRESSIONS FOR THE VELOCITY AND TEMPERATURE DISTRIBUTIONS IN A HYPERSONIC SPHERE WAKE

It is evident, from examining the mathematical expressions for probe current given in the previous section, that in addition to depending on the ion density, the current also depends on the electron and ion temperatures (here presumed equal to the neutral temperatures), and in the case of the kinetic theories, on the flow velocity. Now, in this connection, the wakes of 2.7 inch diameter hypersonic spheres have been extensively studied at DREV (Reference 13), as a result, experimental temperature and velocity data are available. Two independent techniques have permitted the measurement of the distribution of velocity in the direction parallel to the wake axis: that of the transverse electrostatic probe survey array (Reference 1) and that of the sequence of sparks (Reference 13). An important contribution of the spark technique has been to establish that the radial profiles of velocity have approximately the form of a gaussian distribution,

$$V/V_\infty = (V_o/V_\infty)\exp(-(R/r)^2)$$

where

V_∞ is the velocity component parallel to the wake axis
V_o is the value of V on the wake axis
V_∞ is the velocity of the projectile
R is the radial coordinate
r is the width at $V/V_\infty = V_o/V_\infty e$.

As a result the velocity field in the wake is completely determined if the behaviors of V_o and r as functions of the normalized axial distance are known. Following the spark velocity analysis, Sévigny et al. (Reference 1) have also used the gaussian distribution to fit radial distributions of velocity estimates obtained from pairs of ion probes. Their results are summarized in Figures 4 and 5 which give the behavior of the velocity wake radius and the wake velocity on the axis for the firings of 2.7 inch diameter spheres at 14,500 feet/second in nitrogen atmospheres at 7.6 and 20 torr respectively. In the figures, the open circles represent normalized velocity radii (r_v/D) while the solid circles represent normalized wake velocity on the axis (V_o/V_∞).

The other physical variable which must be known before the ion density can be calculated is the temperature. The temperature can be deduced from the mass density distribution if one assumes that the pressure is constant in the wake and that the compressibility factor is unity. Dionne and Tardif, utilizing the electron beam fluorescence probe technique (Reference 14) have measured the radial profiles of mass density behind 2.7 inch diameter spheres flown at 14,500 feet/second in a nitrogen atmosphere at 7.6 torr. From these measurements, and assuming the temperature excess (T/T_∞-1) to be gaussian, they have determined the behavior of the temperature excess on the wake axis (T_o/T_∞-1) and the wake temperature radius r_T/D, as shown in Figure 6 (Reference 15). Unfortunately the electron beam technique did not allow measurements to be made at higher pressures. In order to make calculations of ion density levels at 20 torr, we have been obliged to use the same (7.6 torr nitrogen) temperature data

Obviously a great simplification in programing is possible if tables of experimental data can be replaced by analytical expressions. Accordingly, an analytical expression of the form

$$\text{Log}_{10}(Q) = a + b\ [\text{Log}_{10}(X/D/c)]^2$$

has been found to represent reasonably well the velocity (Reference 1) results and the temperature (Reference 15) results shown in Figures 4 - 6. The value of the constant 'c' corresponds to the axial coordinate of the point of origin for the curve. The values of the constants a and b were determined by the method of least mean squares. The values of the three constants a, b, and c are given in Table IV for each of the profiles shown in Figures 4 - 6. For values X/D smaller than c, it is assumed that $Q = 10^a$, or that the profiles are flat in this region. This is a crude simplification; however, it is not necessary to improve upon it given the small amount of experimental data involved.

6.0 EXPERIMENTAL RESULTS

Because of the statistical character of turbulence, the determination of any fluctuating physical quantity associated with the turbulent wake of a hypersonic projectile requires many independent observations. To carry out a measurement on the ballistic range requires the repetition of the experiment many times under the same experimental conditions. At the same time, depending on the nature of the quantity under study, it may happen that certain critical conditions are difficult to reproduce. This is a problem when dealing with charge density. The charge density levels depend on the composition of the gas filling the range, the cleanliness of the projectile, and at DREV, on the cleanliness of a 400 foot long, 10 foot diameter flight chamber, while the current collected can be affected by the cleanliness of the probes. All of these factors are difficult to control. Unless one has a means of selecting or rating the rounds, one must expect to encounter large variations in

the measured ion density from one round to another. The scattering of the measurements is much stronger in the case of ion density than it is, for example, in the case of measurements of convection velocity (Reference 1). It is necessary, therefore, to exercise care before deciding to include any particular round in the analysis.

All of the rounds considered here have been obtained by firings in nitrogen atmosphere, either at 7.6 torr or at 20 torr. However, there are considerably more results available at 7.6 torr than at the higher pressure, a gross number of about 20 rounds, in fact. This large number of rounds makes it possible to discard immediately any round whose mean behavior appears doubtful. Such abnormal behavior could result from a spall on the projectile (which was not detected on the flash X-ray system) or by the presence of a piece of sabot following behind the projectile in its wake as it passes the experimental station. Frequently, one can spot anomalies directly from the probe signals, but this is not an infallible method, particularly if the problem arises from range atmosphere contamination. Two other independent equipments whose results depend on charge density levels in the wake provide the means to assess the quality of the probe results. One of these is a double-beam microwave interferometer while the second is a six-channel scatterometer used to study the distribution of microwave radiation scattered from the ionized wake. Comparison of the results on a round from among all the ionization-sensitive equipments permits the detection of probably most of the anomalies which may be present during any experiment. (One unresolved problem is that both microwave equipments are downrange of the ion probe experimental station, so that an anomaly due to a fragment for example, might no longer be present when the projectile passes the other stations). On the basis of these comparison, the number of rounds at 7.6 torr was reduced to 14 rounds for analysis. However, following a preliminary study, another three rounds were pruned because of an apparently peculiar behavior, thus leaving eleven for analysis. Among these three, two showed mean current levels which were about an order of magnitude higher than the mean of the other rounds, while the decrease of current with the increase

of axial distance behind the projectile was abnormally slow. The third rejected round showed a similar behavior to those of the other two rejected rounds, although the effects were less pronounced. The rejection of these three rounds could be argued as being somewhat arbitrary; in fact, this decision seems the only logical procedure, given the discussion above.

If it was possible to exercise a degree of fastidiousness in the selection of those results which were to be included in the analysis at 7.6 torr, unfortunately it was not so easy to be selective in the case of the results at 20 torr. In effect, because of the small number of rounds constituting the results, it was felt necessary to keep in the analysis some which were not considered perfect. Perfection is a relative term; however, none of the rounds retained in the analysis exhibited a behavior similar to that found in the three rejected rounds from the 7.6 torr results. To the contrary, the scatter of these results is completely random. The number of rounds included in the analysis at 20 torr amounted to six.

Although few papers are available concerning point measurements of charge density in the wake (References 8 - 10), these do seem to be in agreement in attributing to the radial profiles of ion density (References 8, 9) and electron density (Reference 10), an approximately gaussian distribution. This observation is confirmed, a posteriori, by the results of the present paper. Our analysis of the ion density estimates made with the survey array is thus a repeat of the type of analysis performed in the case of the convection velocity estimates described in Reference 1. The measurements belonging to the same pressure are first grouped into axial bands according to the combination 60-30-60 (Reference 1), where the first number designates the axial coordinate of the first band, the second is the distance between the centers of adjacent bands, and, finally the third is the width of the band. Since the third number is larger than the second, it follows that adjacent bands are partially overlapping. We take for granted here that the size of the axial bands has but little

influence on the final results of the analysis, as we have shown in the case of velocity measurements (Reference 1). The combination 60-30-60 is the preferred choice here over others (Reference 1) because it offers resolution (a radial profile is obtained at every 30 diameters behind the projectile) as well as statistical precision.

The radial profiles defined by this choice are fitted individually by the gaussian function

$$n_i = n_o \exp(-(R/r_i)^2)$$

using the method of least mean squares. Here

n_i is the ion density at any point in the wake,
n_o is the ion density on the wake axis at the same X/D

and

r_i is the ion density radius of the wake.

Figures 7a and 8a show one radial density profile for each of the two range pressures of 7.6 and 20 torr in nitrogen. The ion density, normalized by the ion density on the wake axis (n_i/n_o), is plotted as a function of normalized radial distance from the wake axis (R/D). The open circles represent independent estimates of the ion density, while the solid circles represent values averaged over radial bands of width $\Delta(R/D) = 0.2$. The continuous line is the result of the fit to the data and shows the general trend of the measurements. Evidently the radial distributions of ion density conform to the gaussian curve. As well, it should be remarked that the gaussian character of the profiles at 20 torr is very pronounced even at relatively large axial distances behind the projectile (Figure 8a). Generally, it appears that the radial profiles at 7.6 torr (Appendix B) lose their gaussian appearance at smaller axial distances behind the sphere than do the profiles at 20 torr (Appendix C). (We will discuss later the effect of this on the results).

Concerning the precision of the radial profile fits, the sole method of evaluating this consists in obtaining the contours of confidence (References 1, 16). Figures 7b and 8b show four such contours surrounding a point (indicated by a cross) whose coordinates are the fitted values of the parameters r_0 and r_i/D previously defined. As in the case of convection velocity (Reference 1), we will use here the 90% confidence contours in specifying the error limits.

The behavior of the ion density levels along the axis of the wakes of 2.7 inch diameter spheres flown at 14,500 feet/second in nitrogen atmospheres, as predicted by various theories, are exhibited in Figures 9 to 13. The first two, Figures 9 and 10, concern the predictions of the static theories, those of Zakharova et al., Su and Kiel, and Schulz and Brown, at 7.6 torr and at 20 torr, respectively. The results shown in these two figures possess certain characteristics in common. Apparently, the theory of Zakharova et al. predicts a value of n_0, the axis value of ion density, which is appreciably larger than that predicted by the two other static theories. In fact, this is simply because the theory of Zakharova, as originally derived (Reference 2), is in error by a factor of about 5-8 (Reference 11). When the proper correction is made, the 'modified' theory of Zakharova tends to coincide with that of Su and Kiel, except that the theory of Su and Kiel was derived assuming a thin sheath, whereas that of Zakharova contains a correction for the effect of sheath thickness. (Allowance for the effects of sheath thickness leads the 'modified' Zakharova theory to predict somewhat lower ion density levels than Su and Kiel theory). In this paper, we have preferred to reserve the name 'Zakharova theory' for the original theoretical development as published by Zakharova et al.

Having disposed of the problem of explaining the larger values of ion density predicted by Zakharova theory, we now turn to other effects. It is evident that the wake ion density calculated from the theory of Su and Kiel (and consequently from the 'modified' theory of Zakharova as well) does not differ greatly from the ion density deduced from the theory of

Schulz and Brown. The agreement between the results of the application of Su and Kiel theory and Schulz and Brown theory is even better at higher pressure (Figure 10). A final observation concerning the ion density deduced from the 'static' theories is that, with the possible exception of the theory of Su and Kiel at 7.6 torr, the axial value of the ion density appears to decay over the major portion of the axial distance according to a law of the form

$$n_o = (X/D)^{-2}$$

which is valid to about 400 diameters behind the projectile. (It is interesting to note that a two-body recombination scheme, independent of temperature, leads to a decay law for the charge density which varies as $(X/D)^{-2}$ (References 10, 17) and which implies that diffusion of electrons does not play an important role in the near wake (Reference 17)). At axial distances greater than X/D = 400, there is an apparent flattening of the decay, barely perceptible at 20 torr, but very evident at 7.6 torr. This is almost certainly the result of attempting to measure probe currents down in the noise of the recording system. While the preamplifier-line-driver system was more than adequate, limitations had to be imposed on the sensitivity with which various signals could be recorded because of the lack of an adequate number of recording channels. Probes located near the center of the wake were matched to a recording sensitivity considerably below that used with probes near the edge of the wake, simply because of the desire to record the initial part of the signals and the inability to allocate sufficient numbers of other recording channels to observe the signal behavior at larger axial distances. (The recording compromise has been discussed in some detail in Reference 18).

If we compare the ion density levels along the wake axis at the two pressures, we note that the value of n_o at 20 torr is about an order of magnitude larger than it is at 7.6 torr, for all theories. Another apparent difference is that at axial distances less than 100, the value of n_o stays constant as X/D decreases for the 20 torr case, but

continues to increase as X/D decreases for the 7.6 torr data. (However, this particular effect may not be real. On tho basis of observations on the wake structure (Reference 18), the wake velocity radii (Reference 1), and the wake ion density radii to be discussed later in this report, the wake behind a 2.7 inch diameter sphere at 20 torr is narrower than it is at 7.6 torr. Since the ion probes of the array are situated rather far from the axis at small axial distances, the high electron densities near the axis may be inadequately represented in the radial distributions, and the peak value on the axis may be underestimated, particularly at 20 torr because of the narrower wake width). Again, as previously mentioned, another difference is that at 7.6 torr the ion density on the axis decays with increasing axial distance according to a -2 power law, and apparently reaches a plateau at about X/D = 400, while the presence of a plateau is barely perceptible in the 20 torr results. However, as regards this difference, as previously explained, the probable cause is simple lack of sensitivity in the recording of the probe signals, particularly those from near the center of the wake.

Let us now recall that in addition to treating the probe results with the various static probe theories, we have also employed the kinetic theory of Kulgein and the two kinetic theories of Clements and Smy, for thin sheaths and for thick sheaths. Since the kinetic theories try to take account of the velocity of the ionized medium with respect to probes immersed in it, presumably they should be better adapted than static theories to ballistic range conditions. Figures 11 and 12 show ion density data along the wake axis at 7.6 torr and 20 torr using the various kinetic theories and can be compared with Figures 9 and 10 obtained with the static theories. On comparing the two sets of figures, one realizes immediately that the axial profiles obtained with the kinetic theory have almost the same appearance as those obtained with the static theories: There is the same linear region from about 100 to 400 diameters where the axis value of the ion density decreases with axial distance as a -2 power law. Again, the 20 torr results indicate a plateau at small axial distances less than 100 diameters, while the 7.6 torr results show

a plateau for X/D exceeding 400. A discussion of these observations has already been given in the case of the static theories. In the case of the kinetic theories, the effect of pressure is such that the level of ionization at 20 torr is about 5-10 times that predicted at 7.6 torr.

What really distinguishes the predictions of the kinetic theories from the static theories is the difference in the calculated levels of ionization density. (Here we must remind ourselves to ignore the Zakharova theory results in the static case, because of the errors in the Zakharova theory which, when corrected, cause the Zakharova results to lie close to the results of Su and Kiel theory). Ignoring Zakharova theory, then, the kinetic theories predict a level of ionization which is a factor of 10 lower than the static theories at 7.6 torr. At 20 torr, the difference is even slightly larger than it is at 7.6 torr. One should not be too shocked by the size of these differences. It is now recognized (Reference 6) that the static theories are probably grossly inadequate for probes immersed in a flowing collision-dominated plasma.

The calculation of the confidence contours such as those given in Figure 4b and 5b is very time-consuming. For this reason we have limited ourselves to calculating these contours for only one theory out of the six discussed previously, namely, the thin sheath theory of Clements and Smy. Even so, since we are dealing with the same experimental measurements, the error limits determined with one theory should be representative of the error limits pertaining to the other theories. Figure 13 shows two of the profiles previously given in Figures 11 and 12 but with the addition of horizontal and vertical bars on many of the points to specify the indicated precision. As previously mentionned the vertical lines are based upon the 90% confidence contours. The horizontal bars represented an imprecision of ± 15 diameters in the value of X/D, resulting from the fact that the mean currents are evalued from 0.5 millisecond long segments of probe signal. This has been discussed in more detail in a previous report (Reference 1). From Figure 13, we can state in the way of conclusion, that the values of the ion density along the wake axis are fairly well define.

The ultimate interest in the present research lies obviously in the comparison of the ion density levels estimated through the employment of various probe theories with the ionization levels obtained by other techniques. At 7.6 torr, information concerning the electron density distribution is available from measurements on a small number of rounds made with a dual channel microwave interferometer. In this technique (Reference 19), the two simultaneous phase shift measurements obtained with the two channels are used to solve for the amplitude and radius of the assumed gaussian distribution of electron density in the wake. In addition, one 7.6 torr firing has been observed with very fine wire (Langmuir) probe instrumentation (Reference 20). At 20 torr only microwave interferometer results are available.

Figure 14 compares the profile of ion density deduced on the wake axis using the thin sheath theory of Clements and Smy (solid circles) with the electron density on the wake axis obtained by averaging over the results of interferometer measurements on four different rounds (open hexagons) and with the electron density measured by a Langmuir probe situated at a radial distance of 0.78 sphere diameters from the axis of the wake (half-solid circles). All these measurements were obtained with 2.7 inch diameter spheres flown in 7.6 torr nitrogen at Mach 13. Since the atmosphere was nitrogen in these investigations, no electron attachment should occur (Reference 17) and the electron and ion densities in the wake should be comparable. The results (Figure 14) indicate that at 7.6 torr and an axial distance of 100 diameters behind the sphere, the ion density level predicted by the Clements and Smy thin sheath theory is a factor of five too high, based on the assumed correctness of the interferometer data. This is a disappointing result. However, at higher axial distances, the results seem to tend to a better agreement: In the axial distance range from 240 to 400 diameters, the results of all the various techniques agree within a factor of two. It will be noticed, as before, that the ion probe results indicate a kind of plateau in ion density at axial distances greater than 400 diameters, while the electron density levels deduced from the Langmuir probe continue to decay with axial distance. This fact confirms the previously expressed explanation of the apparent flattening of the ion density decay.

At 20 torr, only interferometer electron density results are available with which to compare the ion density levels inferred from the ion probe theories. Contrary to what might be expected, the difference between these two sets of data (Figure 15) is larger at higher pressure. At an axial distance of 100 diameters, the ion density levels predicted by the Clements and Smy thin sheath theory are about 15 times higher than the electron density inferred with the interferometer equipment, while at 400 diameters, the difference is about a factor of seven. The interferometer data at 20 torr in nitrogen were obtained by averaging over the results of three separate rounds, but seem reasonably consistent with the interferometer data at 7.6 torr. The results of the comparison of the predictions of the probe theory with the measurements of the interferometer equipment must once again be classified as disappointing. It would seem indeed to confirm that 'The Theory' of electrostatic ion probes does not yet exist.

Before terminating the discussion of the ion density levels, one additional point can be added. Certain US laboratories tend to present the results of their charge density measurements (via cavities or interferometers) in the form where the ion or electron density is integrated along a line traversing the center of the wake in a direction perpendicular to the axis. In order to facilitate the comparison of the present results with those of other laboratories we have calculated the value of the following integral (Reference 21)

$$\int_{-\infty}^{\infty} n_o \, e^{-(R/r_i)^2} dR = \sqrt{\pi}\, n_o r_i = n_i D_p .$$

The results of these calculations are given in Figures 16 and 17. Generally the bahavior of the profiles of $n_i D_p$ (Figures 16, 17) are not unlike those for n_o, the ion density level on the wake axis (Figures 9 - 12). However, there are slight differences as concerns the slope of the decay in the so-called linear region (between 100 and 400 diameters behind the projectile). For example, the slope of the $n_i D_p$ curve at 7.6 torr is minus 1.5, while that for n_o is minus 2 (Figure 16). However, at 20 torr, both the $n_i D_p$ and the n_o curves decay with axial distance in accord with a slope of minus 2 (Figure 17).

In addition to the behavior with axial distance of n_o, the ion density on the wake axis, the fitting of the radial ion density profiles deduced from the various theories provides equally the behavior of the ion density radius of the wake. Figures 18 and 19 show the behavior with axial distance of the ion density wake radius predicted by the kinetic theories at pressures of 7.6 torr and 20 torr respectively. The error bars on the two figures have been defined in the same manner as those shown in Figure 13. The solid line representing the equation $0.4\ (X/D)^{1/3}$ has been found to represent the wake core width as measured from schlieren photographs of the wakes of Mach 13 spheres at various pressures (Reference 22). At 7.6 torr it has not been possible to determine the ion density wake radius beyond X/D = 400 diameters, because of the strong scattering of the data (Figure 18) which reduces to almost nil the precision of the estimate of the parameter r_i. (In other words the intervals of confidence tend to extend to infinity). This phenomenon is undoubtedly related to the flattening in the profile of the axis ion density observed in the 7.6 torr results when X/D exceeds 400 (Figures 9 and 11). At the higher pressure of 20 torr, the ion density radius of the wake remains defined until almost 1000 diameters behind the projectile (Figure 19). However, in this case, the precision of the results is impaired because the number of measurements available is too small.

For purpose of comparison, Figure 20 summarizes the results obtained at 7.6 torr and at 20 torr concerning the radius of the ion density distribution in the wake of a 2.7 inch diameter sphere flown at Mach 13. Obviously, the profile corresponding to the ion radius at 20 torr ($P_\infty D$ = 54 torr inches) falls below the profile at 7.6 torr ($P_\infty D$ = 20 torr inches). The shift in these results is systematic and statistically significant. The direction of the shift indicates that an increase in ambient pressure entails a shrinking of the size of the ion density wake. At 7.6 torr, as well as at higher pressures, the size of the ion wake is notably smaller than the size of the so-called schlieren wake. Conclusions similar to these have been drawn by Heckman and Sévigny in their study of the wake structure behind hypersonic spheres (Reference 18).

In the preceding paragraphs, we have not referred to any particular theory in discussing the behavior of the radius of the ion density distribution in the wake. This is because the three kinetic theories predict the same values for the wake ion radius. As for the predictions of the static theories, these indicate an ion radius somewhat larger than do the kinetic theories. Nevertheless, since these theories do not really correspond to reality, in the sense that they completely neglect plasma flow velocity, we have preferred to ignore the static theory predictions in this case. For those readers who wish to further examine the above statements, a listing of results is given in Appendix A.

Figures 21 and 22 compare the radii of the ion density distributions in the wake from Figures 18-20 with the radii of the electron density distributions as deduced from the dual channel interferometer equipment, at 7.6 and at 20 torr respectively. At both pressures the ion density radii are significantly lower than the interferometer electron density radii. The interferometer results are the result of averaging over four rounds at 7.6 torr and three rounds at 20 torr. In the case of these charge density radii we are inclined to put more confidence in the ion probe data. The equation which defines the electron density radius is very nonlinear (Reference 20) and the results are probably biased towards overestimation of the size of the electron density radius.

7.0 CONCLUSION

The spatially-resolved distributions of charged particles in hypersonic turbulent wakes are of interest for the theoretical modeling of such flows, and they are equally of interest for explaining the scattering of microwave energy from wakes. This report is a description of the results of a major research effort undertaken to determine experimentally, through the use of electrostatic probes and existing probe theory, the levels of ion density in the turbulent wakes behind 2.7 inch diameter titanium spheres flown at 14,500 feet/second in a ballistic range filled with nitrogen, at 7.6 torr and at 20 torr.

The major problem encountered in this work is that concerned with the theoretical interpretation of the current seen by an electrostatic probe in terms of ion density. During the past few years, many theoretical interpretations of the current to an ion probe have been proposed. These can be divided into two main categories: the 'static' theories which do not consider the flow velocity of the plasma in which a probe is immersed and the 'kinetic' theories which attempt to account for the effects of the flow velocity. Generally speaking, the theories indicate that the current collected by an ion probe of convenient dimensions is not uniquely dependent on ion density, but also depends on such physical variables as the temperature, pressure, probe potential, and in the case of the kinetic theories, on the bulk velocity of the medium. Where the 'problem' arises is that the probe theories differ in their predictions of the details of the dependence of the probe current on the various physical variables listed above.

A practical problem of considerable consequence is that the application of the various theories cannot be carried out unless the required velocity and temperature data for the experimental medium are known. The work described in this report has benefited greatly by being a sub-portion of a much larger research program in turbulent wakes; in the course of this program the wake velocity and temperature distributions needed to apply the various probe theories have been experimentally determined by our colleagues and ourselves.

Three static theories for electrostatic probes and three kinetic theories have been applied to the mean current data obtained in the wake by means of a transverse survey array of cylindrical ion probes. In each case, the theory has been applied to the current measurements to construct a radial distribution of ion density estimates. These radial distributions have been fitted with gaussian curves by the method of least mean squares. Two parameters of the ion density distributions are determined: the ion density on the axis of the wake and the ion density radius of the wake.

If we consider the results concerning the ion density on the wake axis, we find that the static theories predict ionization levels which are an order of magnitude larger than the kinetic theories at both 7.6 and 20 torr. In turn the kinetic theories predict ion density levels which are higher than the electron density levels measured with a microwave interferometer equipment. At 7.6 torr, the kinetic theories seem to be about a factor of five too high at 100 diameters behind the projectile, but at larger axial distances (240-400 diameters) the ion density results of the ion probes, and the electron density results of the interferometer as well as the results of a Langmuir probe, are all within a factor of two. This is perhaps the most encouraging result to be obtained. However, at higher pressures (20 torr), the difference between the results increases, and the kinetic theory ionization levels are about an order of magnitude higher than the microwave interferometer results.

In actual figures, the kinetic theories predict ion density levels of about 3×10^{10} at X/D = 100 and about 10^{9} at X/D = 400, for nitrogen at 7.6 torr. The corresponding electron density levels from the interferometer are 5×10^{9} at X/D = 100 and 7×10^{8} at X/D = 400. At 20 torr, the kinetic theories predict ion densities of about 1.5×10^{11} at X/D = 100 and about 10^{10} at X/D = 400, while the corresponding interferometer results are 8×10^{9} and 1.5×10^{9} respectively. We can conclude from these comparisons that 'The Theory' of electrostatic probes has yet to see the light of day.

One of the striking conclusions of these investigations is that the predictions of all the diverse theories agree on one point: between the axial distances of 100 and 400 diameters, the ion density on the wake axis decays according to the law $n_0 = (X/D)^{-2}$. In addition to the results concerning ion density levels, interesting information has been generated concerning the widths of the ion density profiles in the wake. Extending from the projectile to an axial distance of 100 diameters, the ion density radii vary slowly and remain smaller than one sphere diameter; after X/D = 100 diameters, the ion radii begin to increase more rapidly. However,

the size of the ion wake is notably smaller than that of the so-called schlieren wake. Over the range of pressures investigated it appears that an increase in ambient pressure entails a shrinking of the size of the ion density wake; the ion density radius of the wake at 20 torr is significantly smaller than the radius at 7.6 torr. The ion radii of the wake have also been compared to electron radii inferred from the interferometer measurements.

It is perhaps useful to point out that the results presented in this report are rendered unique by a number of factors which include the size of the projectile (2.7 inch diameter spheres), the velocity of the projectile (14,500 feet/second), the composition of the atmosphere (7.6 and 20 torr N_2), the region of the wake studied (0 to 1000 diameters), and especially the spatially-resolved character of the measurements. It is consequently impossible to compare these results with those originating from other laboratories (8, 9, 10, 18), and the only results with which comparison is possible are those which have been generated at DREV. In the case of the results at 7.6 torr, the comparison of the ion density levels deduced from the kinetic theories of electrostatic probes with the electron density levels obtained from Langmuir probe and microwave interferometer measurements in quite encouraging. However, at 20 torr the result of a similar comparison is disappointing. As regards the state of development of probe theory, the present results indicate that it is indeed possible to theoretically interpret the mean current collected by an electrostatic probe in a medium as complex as the wake of a hypersonic sphere. However, it would appear that a considerable amount of work remains to be done in order to arrive at a satisfactory theory for such probes.

ACKNOWLEDGEMENT

The authors wish to acknowledge a major contribution by Mr. A. Emond to this research. Other contributors included Miss Carolle Proulx, Mr. Jacques Lemieux, Mr. Gilles Moisan, Mr. Denis Audet, Mr. Phillipe Doyon, and Miss Nicole Bérubé. The manuscript was typed by Mrs Claudette Bigras while Mrs Marie-Paule Kirkwood prepared the figures. The authors are also grateful for the support received from Dr. A. Lemay, formerly Director Aerophysics Division, and for the support from the Aerospace Engineering Section under Mr. P. Solnoky, the Instrumentation Section under Dr. E. Léger, and the Computing Center under Mr. D. Galbraith.

REFERENCES

1. Sévigny, L., Heckman, D. and Emond, A., "Velocity Mapping of Turbulent Wakes of Hypersonic Spheres with Arrays of Ion Probe Pairs", DREV R663 (Unclassified) (to be published).

2. Zakharova, V.N., Kagan, Y.M., Mustafin, K.S. and Perel, V.I., "Probe Measurements at Medium Pressures", Soviet Physics - Tech. Physics, 5, pp. 411-18, 1960.

3. Su, C.H. and Kiel, R.E., "Continuum Theory of Electrostatic Probes", J. Appl. Phys., 37, 13, pp. 4907-10. December, 1966.

4. Schulz, G.J. and Brown, S.C., "Microwave Study of Positive Ion Collection by Probes", Phys. Rev. 98, 6, pp. 1642-49, June, 1955.

5. Kulgein, N.G., "Ion Collection from Low-Speed Ionized Gas", AIAA Journal, 6, 1, pp. 151-53, January, 1968.

6. Clements, R.M. and Smy, P.R., "Ion Current from a Collision-Dominated Flowing Plasma to a Cylindrical Electrode Surrounded by a Thin Sheath", J. Appl. Phys., 41, 9, pp. 3745-49, August, 1970.

7. Clements, R.M. and Smy, P.R., "Electrostatic-Probe Studies in a Flame Plasma", J. Appl. Phys., 40, 11, pp. 4553-58, October, 1979.

8. French, I.P., Arnold, T.E. and Hayami, R.A., "Ion Distributions in Nitrogen and Air Wakes Behind Hypersonic Spheres", AIAA Paper No. 70-87, presented to the AIAA 8th Aerospace Sciences Meeting, New-York, New York, January, 19-21, 1970.

9. French, I.P., Hayami, R.A., Arnold, T.E., Steinberg, M., Appleton, J.P. and Sonin, A.A., "Calibration and Use of Spherical and Cylindrical Electrostatic Probes for Hypersonic Wake Studies", AC-DRL TR69-12, May 1970.

10. Demetriades, A. and Doughman, E.L., "Mean, Intermittency and Turbulence Measurements in a Self-Preserving Plasma Jet", AIAA Paper No. 68-685, presented to the AIAA Fluid and Plasma Dynamics Conference, Los Angeles, California, June, 24-26, 1968.

11. Cantin, A., "The Application of Ion Probes to Wake Diagnostics", DREV R664 (Unclassified) (to be published).

12. Smirnov, "Diffusion and Mobility of Ions in a Gas", Soviet Physics Uspekki, 10, 3, pp. 313-331, November-December 1967.

13. Heckman, D., Tardif, L. and Lahaye, C., "Experimental Study of Turbulent Wakes in The CARDE Free-Flight Ranges", Symposium on Turbulence of Fluids and Plasmas, Polytechnic Institute of Brooklyn, 16-18 April 1968.

14. Dionne, J.G.G. and Tardif, L., "An Application of the Electron Beam Fluorescence Probe in Hyperballistic Range Wake Studies", ICIASF'71 Record, pp. 80-86, presented to the 4th ICIASF Congress, Von Karman Institute, Rhode-Saint-Genèse, 21-23 June, 1971.

15. Dionne, J.G.G. and Tardif, L., (DREV Private Communication)

16. Drapper, N.R. and Smith, H., "Applied Regression Analysis", Wiley 1966.

17. McDaniel, E.W., "Collision Phenomena is Ionized Gases", John Wiley and Sons, Inc., New York, 1964.

18. Heckman, D. and Sévigny, L., "Structure of Turbulent Wakes of Hypersonic Spheres as Inferred with Ion Probes", DREV R669 (Unclassified) (to be published).

19. Heckman, D., Sévigny, L., Doyon, P., Emond, A. and Fitchett, A., "Electron Density Behavior in the Wake of 14,500 feet/second Spheres", DREV R680 (Unclassified) (to be published).

20. Heckman, D., Sévigny, L. and Emond, A., "Absolute Electron Density Measurements in Turbulent Hypersonic Sphere Wakes with Langmuir Probes", (to be published).

21. Hayami, R.A. and Primich, R.I., "Wake Electron Density Measurements Behind Hypersonic Spheres and Cones", AGARD Conference Proceedings CP No. 19 of the Specialists Meeting on the Fluid Physics of Hypersonic Wakes, Colorado Springs, Colorado, May 1967.

22. Lahaye, C., and Doyon, P., "Growth Characteristics of Turbulent Wakes", (to be published).

TABLE I

EXAMPLE OF MESSAGES EXCHANGED BETWEEN OPERATOR AND AUTOMATIC FILM READER

CAL DATA

8199.70
827.00
8364.20
845.00
871.00
884.00
9192.89
92173.88
955.00

-0001	0000	0002	0001
0006	-0002	-0003	0003
-0006	-0012	0005	0015
0001	0003	0004	0012
-0001	-0002	0005	0015
-0001	0002	0006	0013
0002	0003	0005	0010
-0006	0003	0013	0008
0000	0001	0014	0008
0000	-0002	0015	0011
-0002	0002	0017	0010
-0003	0001	0020	0009
0001	0001	0021	0008
0002	0002	0024	0007
0000	0001	0025	0007
0001	-0002	0025	0009
0002	0001	0027	0008
0002	0000	0029	0009
0001	0000	0031	0010
0002	0001	0030	0010
0000	0000	0031	0010
0002	0001	0034	0010
0002	-0001	0035	0012
0001	-0003	0037	0015
-0001	-0001	0038	0017
-0002	-0003	0037	0020
0000	0000	0037	0021
0001	0001	0038	0020

CAL DATA

TABLE II

IDENTIFICATION CODE

CAL (1): Round Number

(2): Camera Number

(3): Projectile Velocity (Diameters/millisecond)

(4): Position of Time Mark Number Zero

(5): Sampling Interval (microsecond)

(6): Axial Distance Corresponding to Analysis Number

(7): Number of Upstream Probe

(8): Number of Downstream Probe

(9): Address of Lower End of 0.5 millisecond Segment of Signal

(10): Address of Upper End of 0.5 millisecond Segment of Signal

(11): Reading Frequency (readings/cm)

(12): Film Velocity (ft/second)

(13): (not assigned)

(14): Analysis Number

(15): Oscilloscope Sensitivity (volt/cm)

(16): R_o (see text)

(17): $\bar{x}$ (see text)

(18): $\sqrt{\overline{x^2}}$ (see text)

(19): $(\bar{y})_o$ (see text)

(20): $\sqrt{(\overline{y^2})_o}$ (see text)

TABLE III

TABLE USED FOR THE INTERPRETATION OF TABLE I

LINE	1	:	512	-	781
LINE	2	:	781	-	1050
LINE	3	:	1050	-	1319
LINE	4	:	1319	-	1588
LINE	5	:	1588	-	1857
LINE	6	:	1857	-	2126
LINE	7	:	2126	-	2395
LINE	8	:	2395	-	2664
LINE	9	:	2664	-	2933
LINE	10	:	2933	-	3202
LINE	11	:	3202	-	3471
LINE	12	:	3471	-	3740
LINE	13	:	3740	-	4009
LINE	14	:	4009	-	4278
LINE	15	:	4278	-	4547
LINE	16	:	4547	-	4816
LINE	17	:	4816	-	5085
LINE	18	:	5085	-	5354
LINE	19	:	5354	-	5623
LINE	20	:	5623	-	5892
LINE	21	:	5892	-	6161
LINE	22	:	6161	-	6430
LINE	23	:	6430	-	6699
LINE	24	:	6699	-	6968
LINE	25	:	6968	-	7237
LINE	26	:	7237	-	7506
LINE	27	:	7506	-	7775
LINE	28	:	7775	-	8044
LINE	29	:	8044	-	8313
LINE	30	:	8313	-	8582
LINE	31	:	8582	-	8851
LINE	32	:	8851	-	9120
LINE	33	:	9120	-	9389
LINE	34	:	9389	-	9658
LINE	35	:	9658	-	9927
LINE	36	:	9927	-	10196
LINE	37	:	10196	-	10465
LINE	38	:	10465	-	10734
LINE	39	:	10734	-	11003
LINE	40	:	11003	-	11272

TABLE IV

VALUES OF THE PARAMETERS a,b,c

Q	$P_\infty D$ Torr-inch	a	b	c
V_o/V_∞	20	-0.948	-0.503	60
r_V/D	20	0.332	0.153	60
V_o/V_∞	54	-0.81	-0.48	60
r_V/D	54	0.2	0.2	60
T_o/T_ω-1	20	0.757	0.388	50
r_T/D	20	0.285	0.083	50

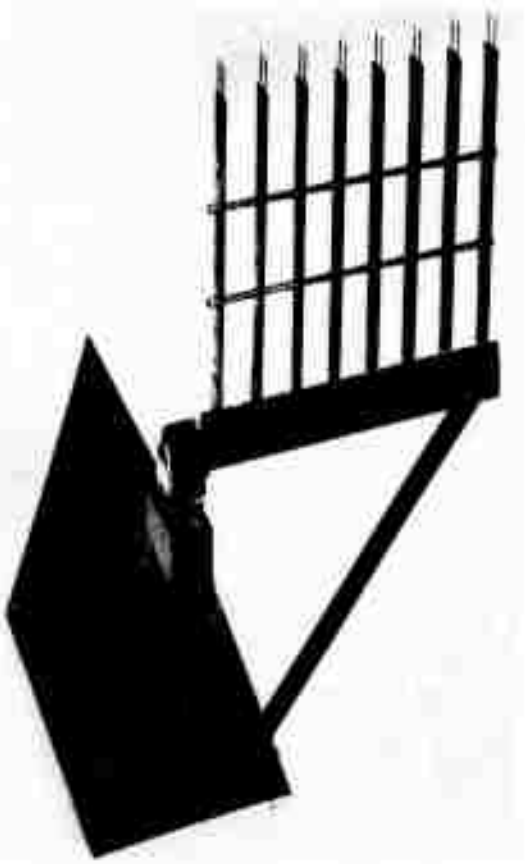

FIGURE 1

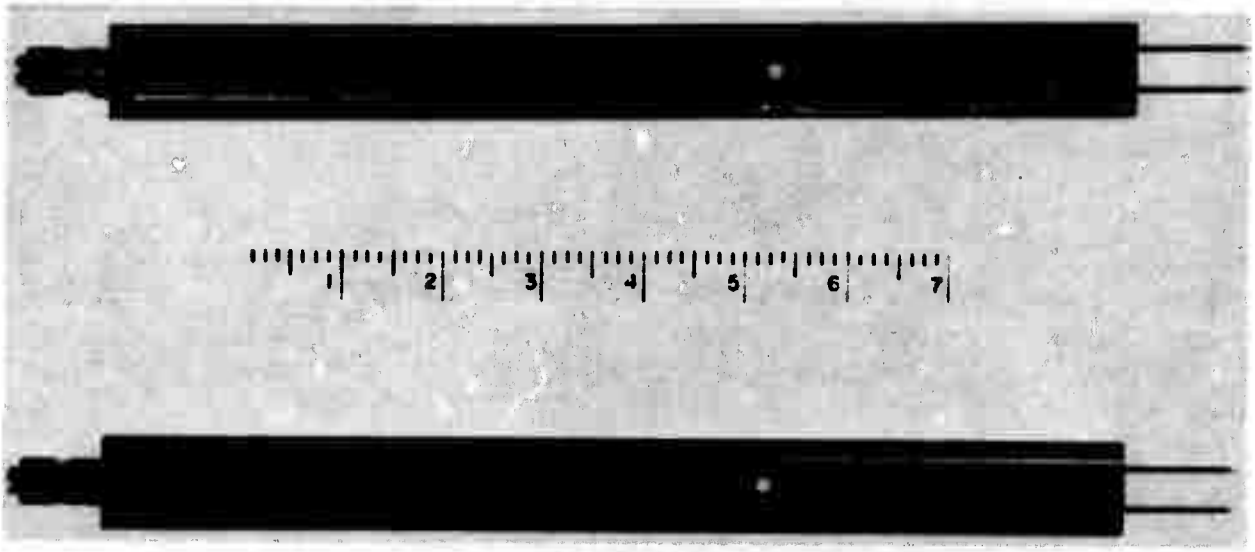

FIGURE 2

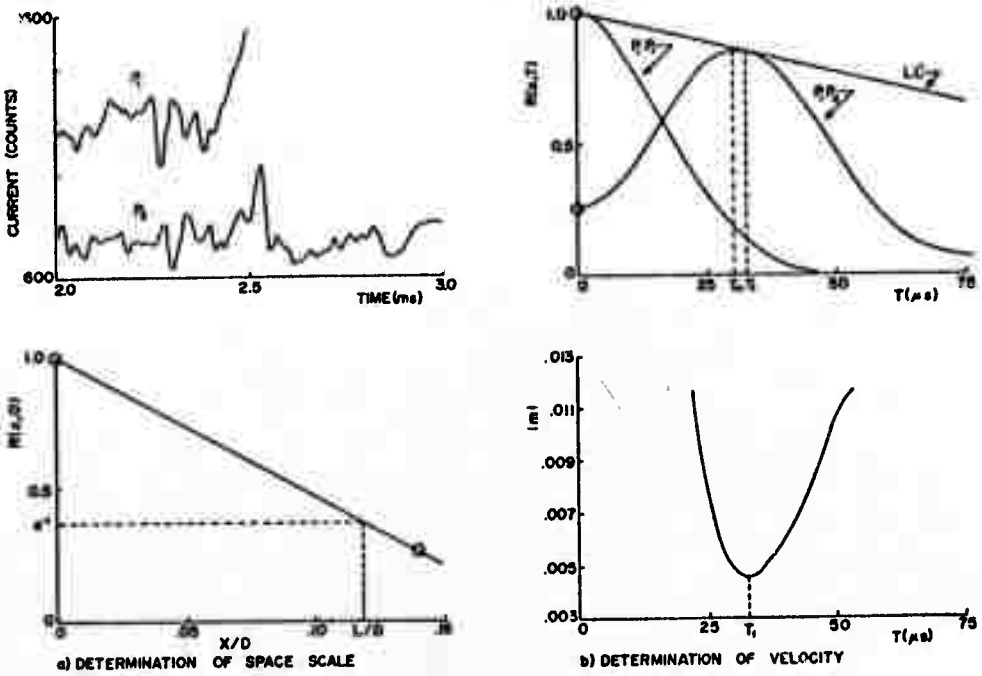

FIGURE 3

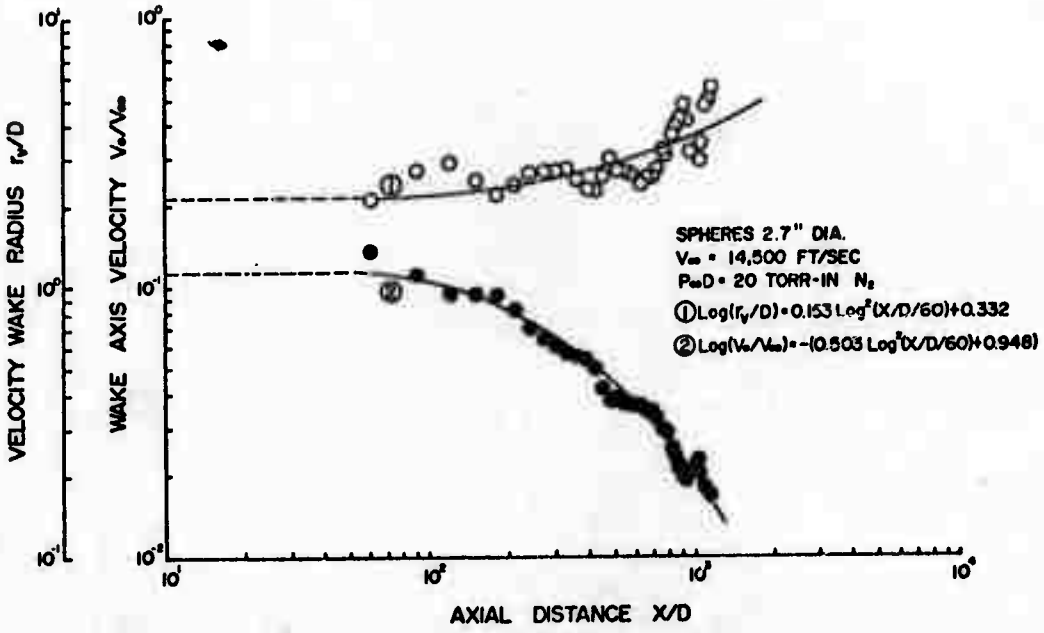

FIGURE 4

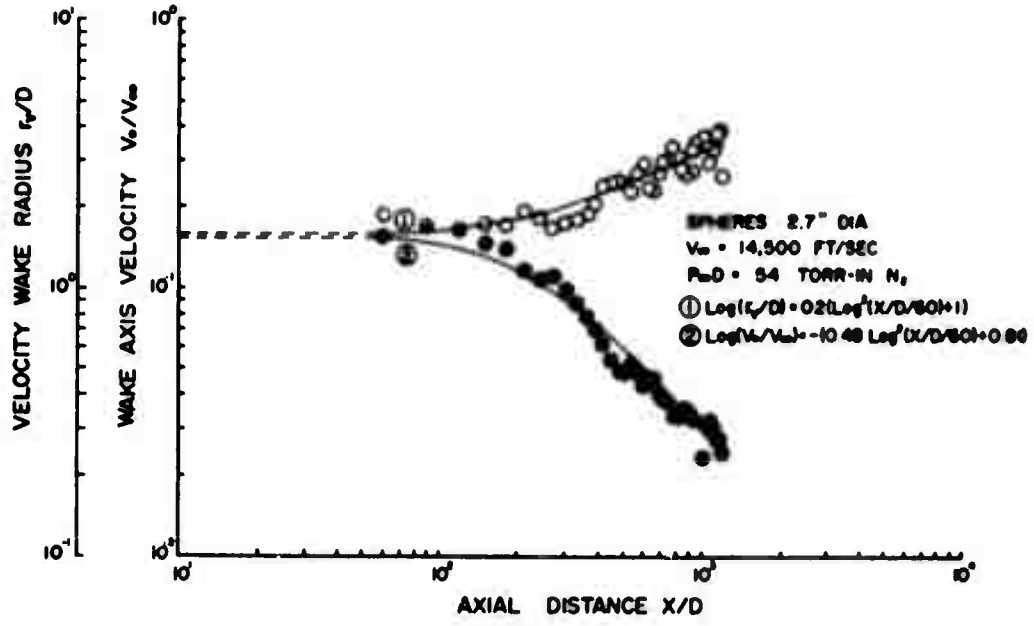

FIGURE 5

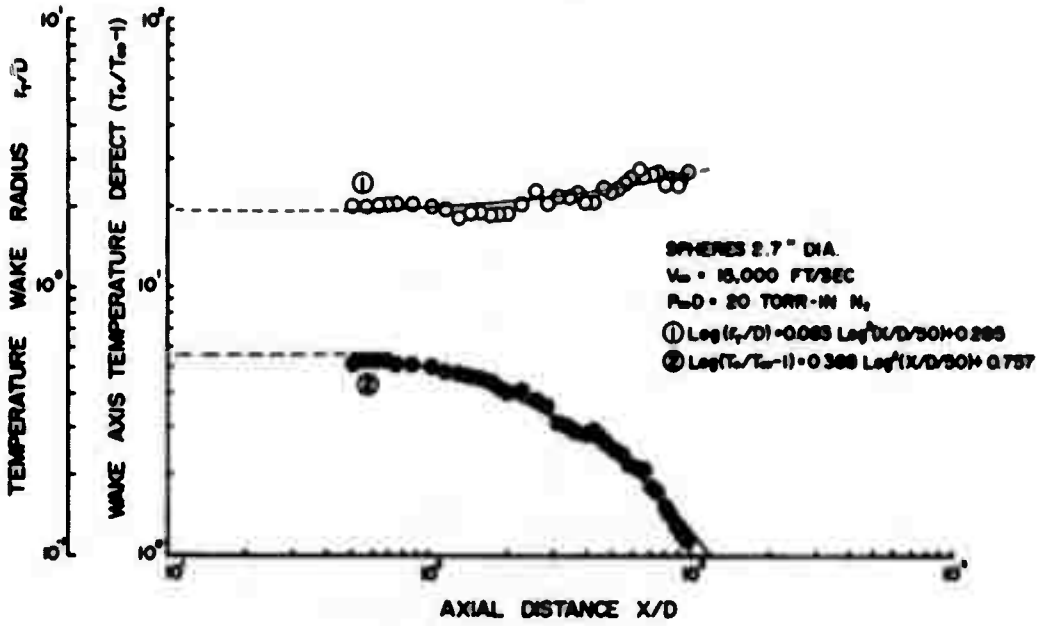

FIGURE 6

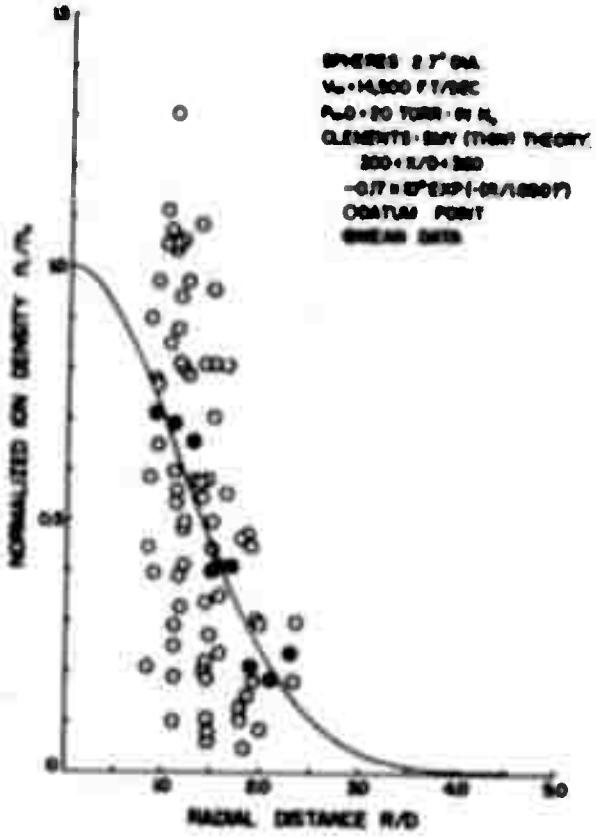
RADIAL DISTANCE R/D

FIGURE 7a

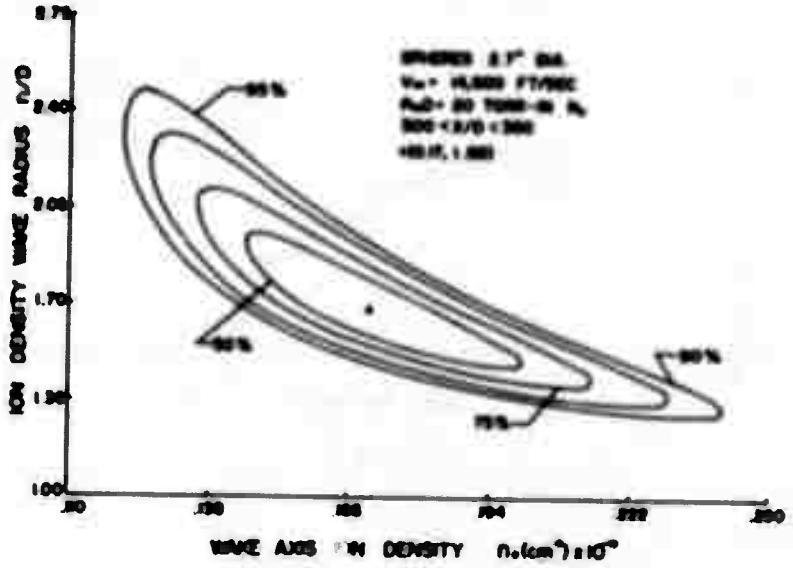
ION DENSITY WAKE RADIUS R/D
WAKE AXIS ION DENSITY

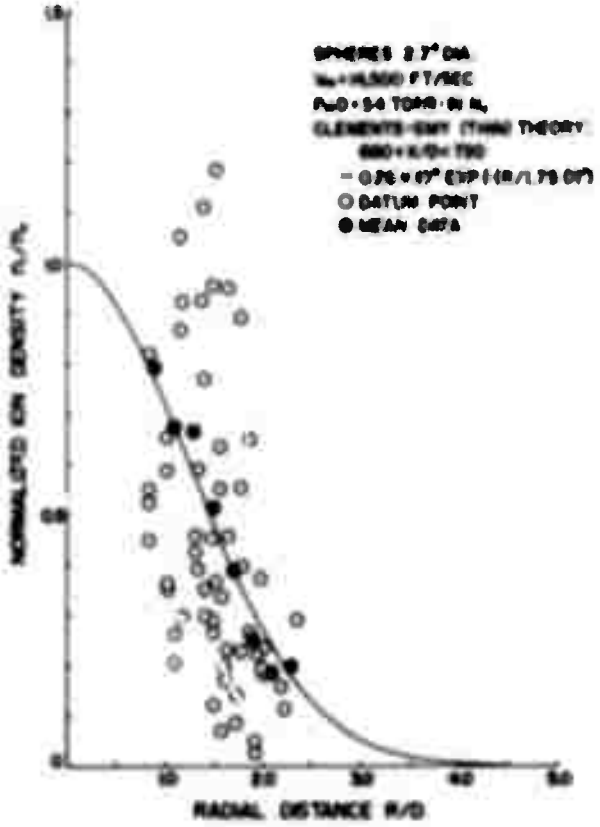

FIGURE 8a

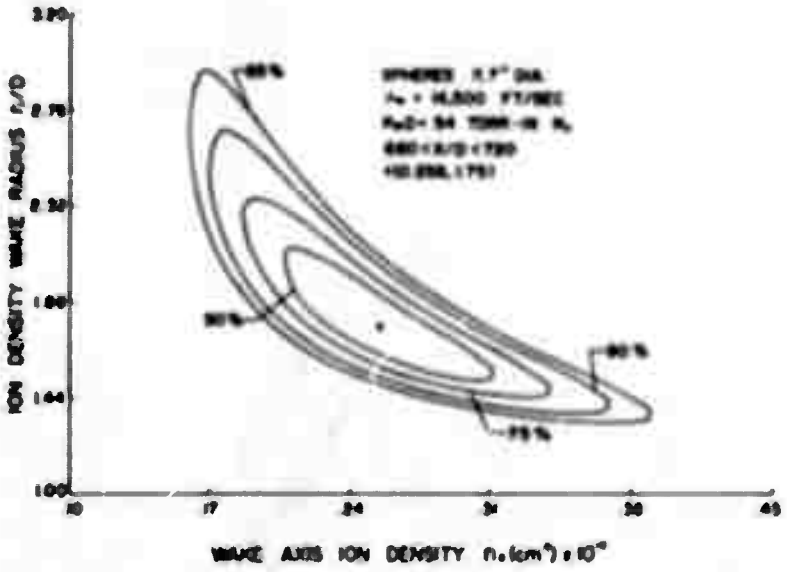

FIGURE 8b

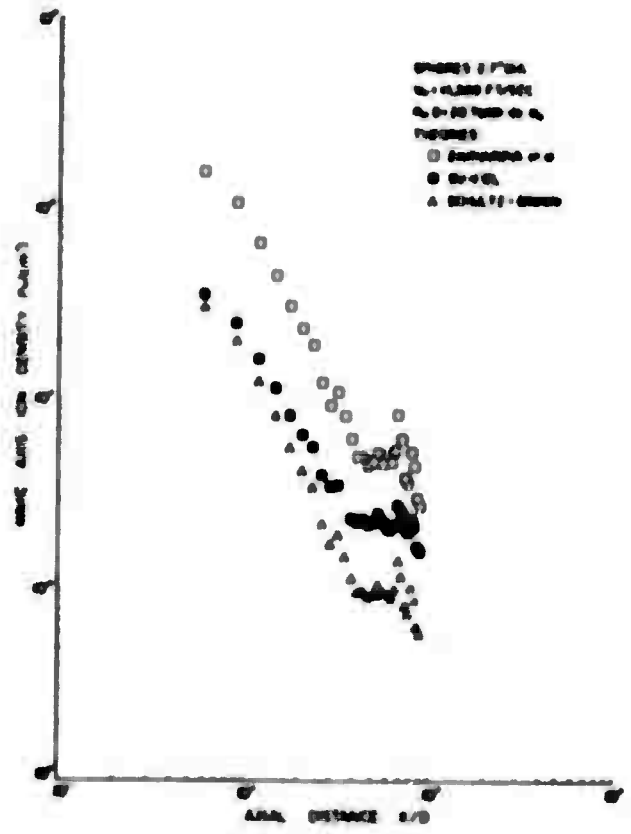

FIGURE 9

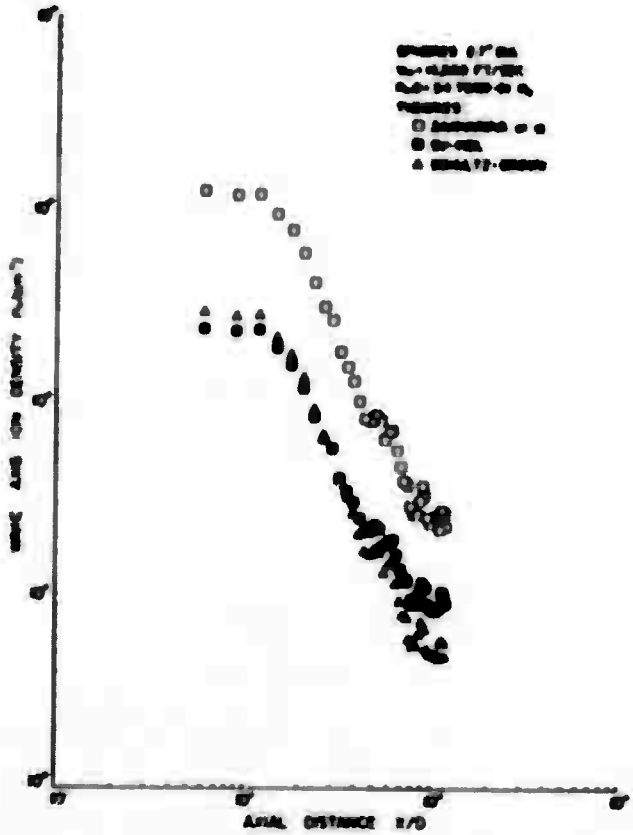

FIGURE 10

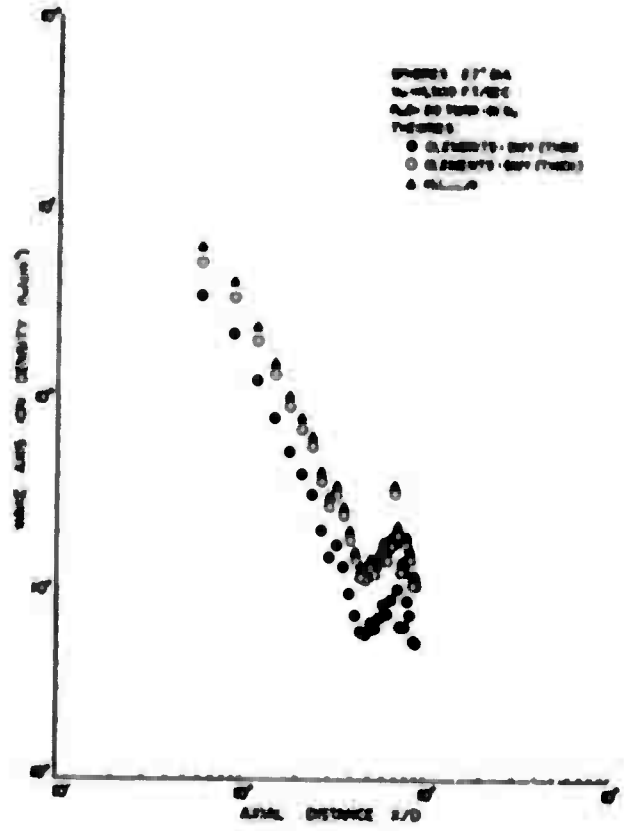

FIGURE 11

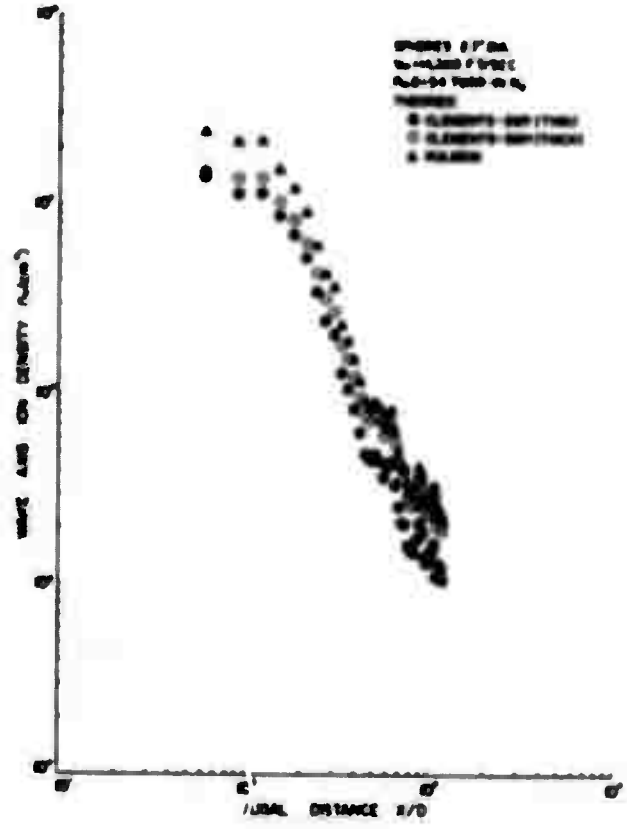

FIGURE 12

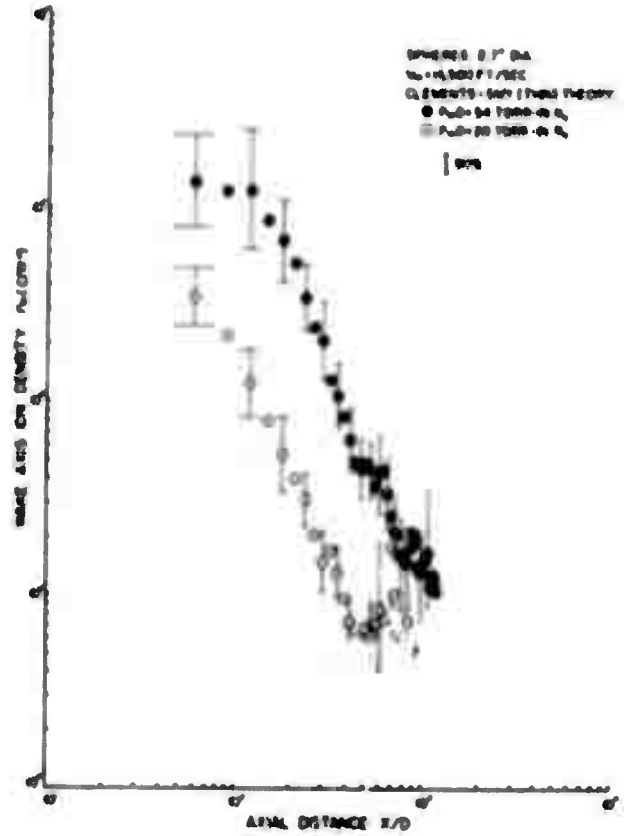

FIGURE 13

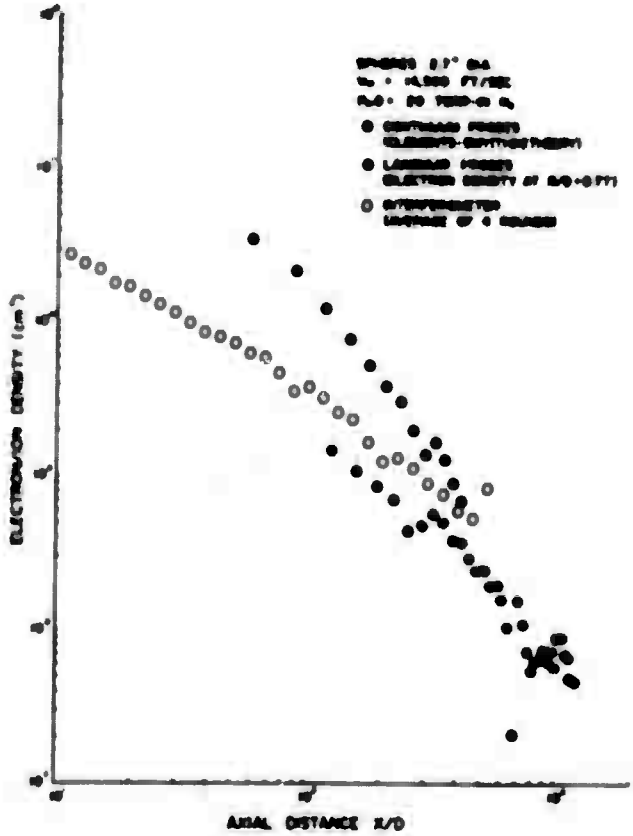

FIGURE 14

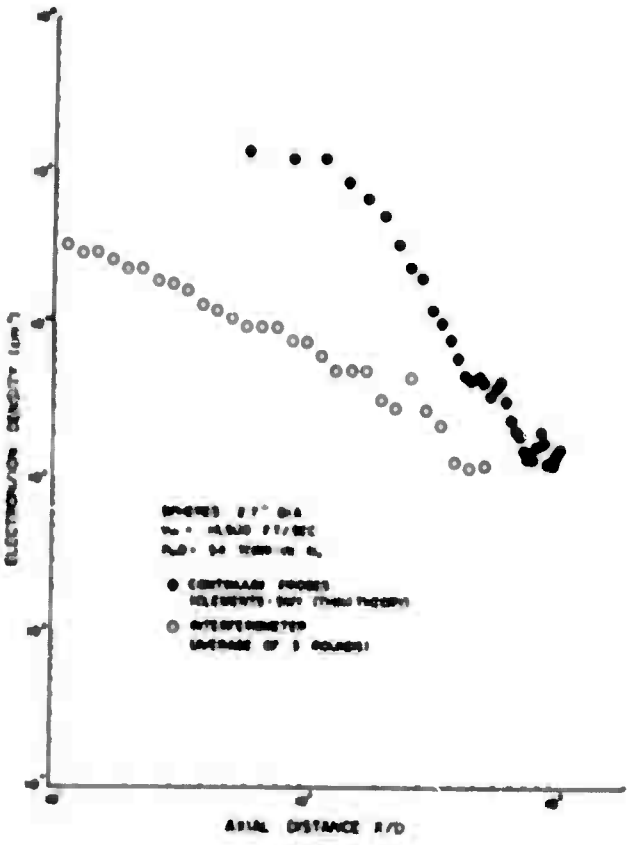

FIGURE 15

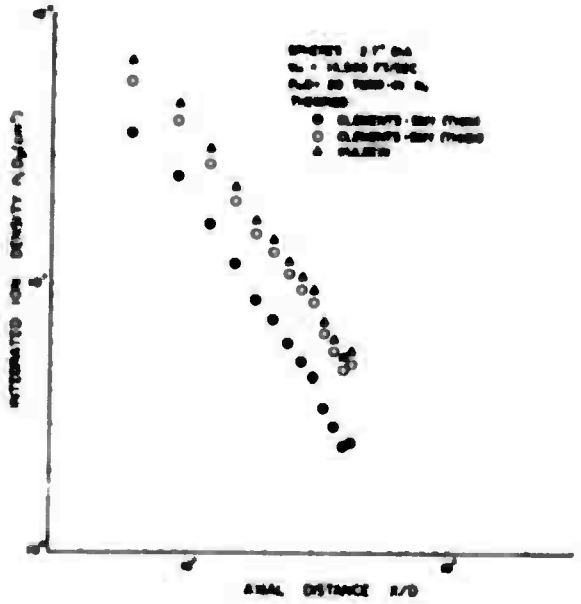

FIGURE 16

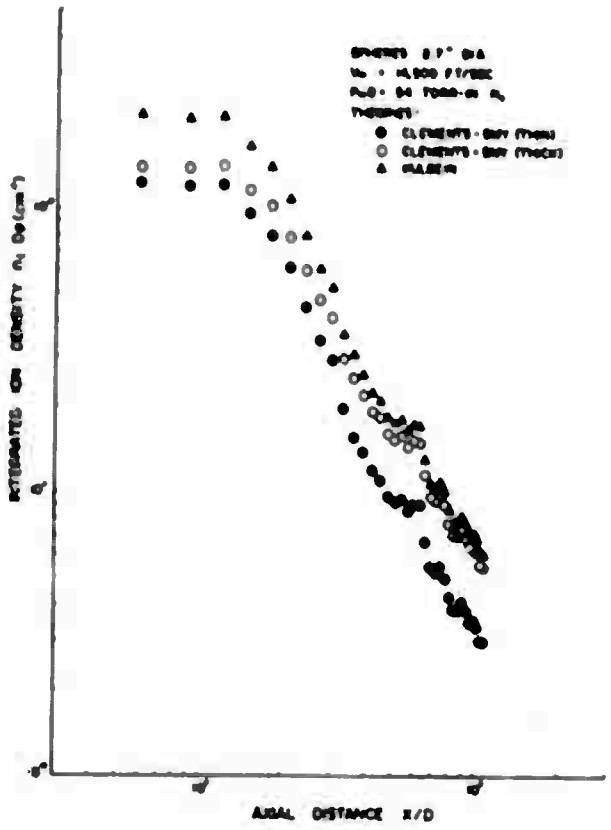

FIGURE 17

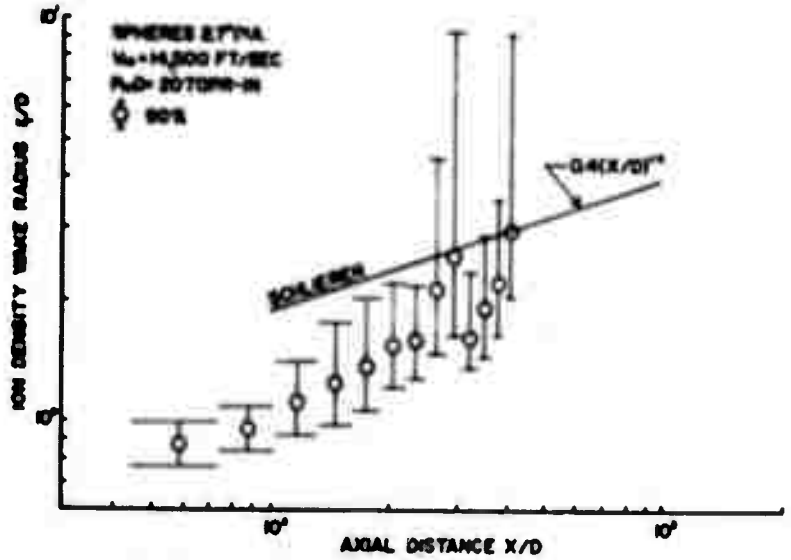

FIGURE 18

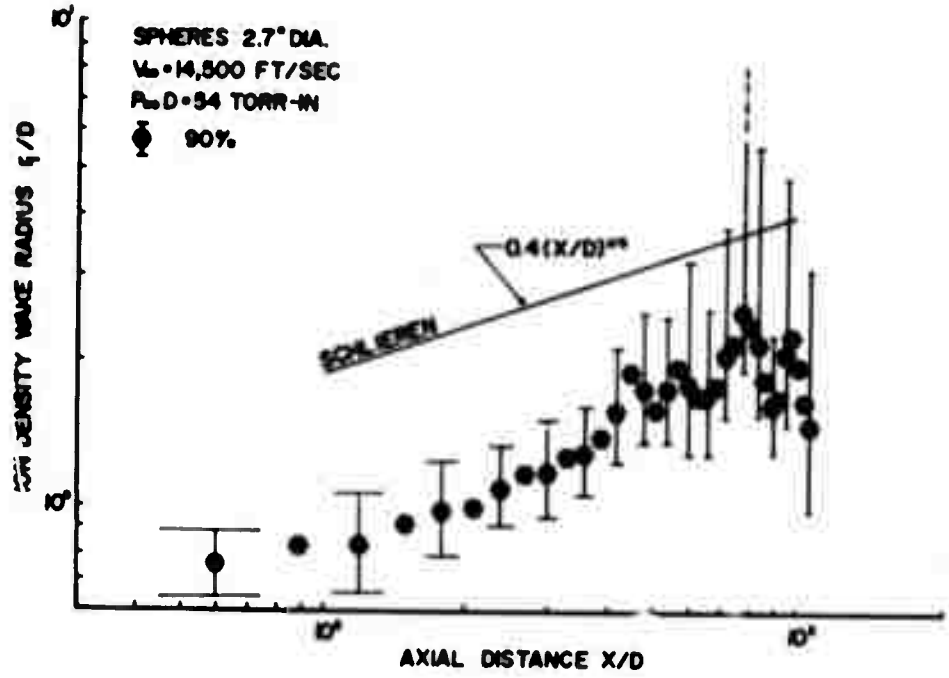

FIGURE 19

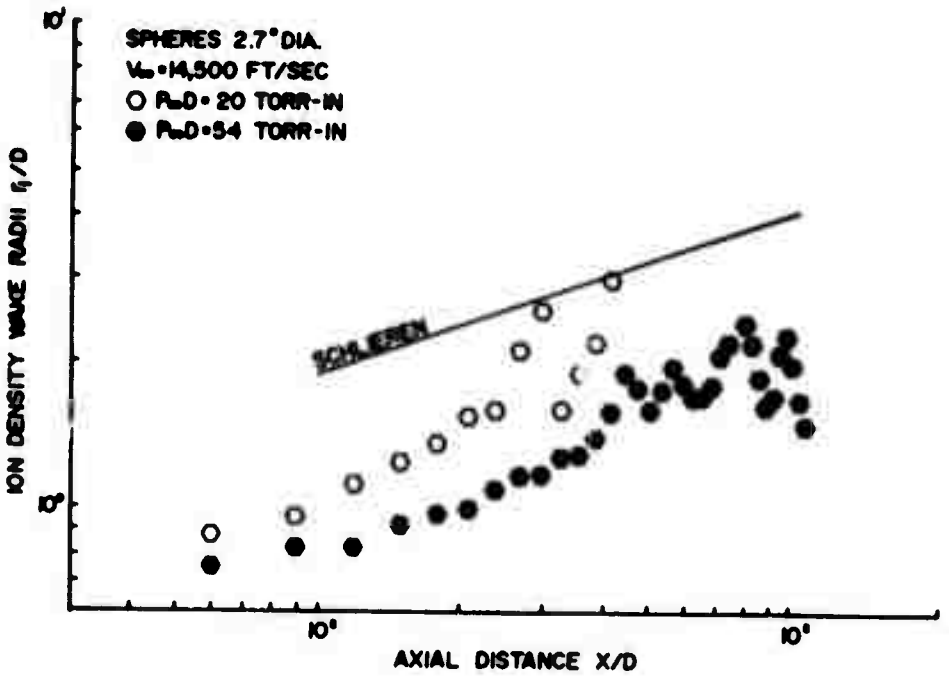

FIGURE 20

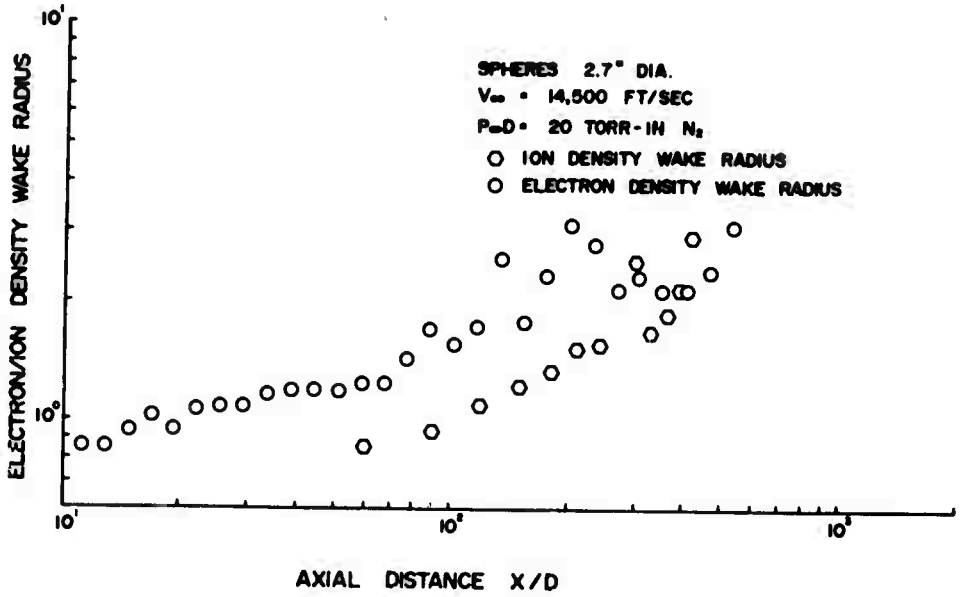

FIGURE 21

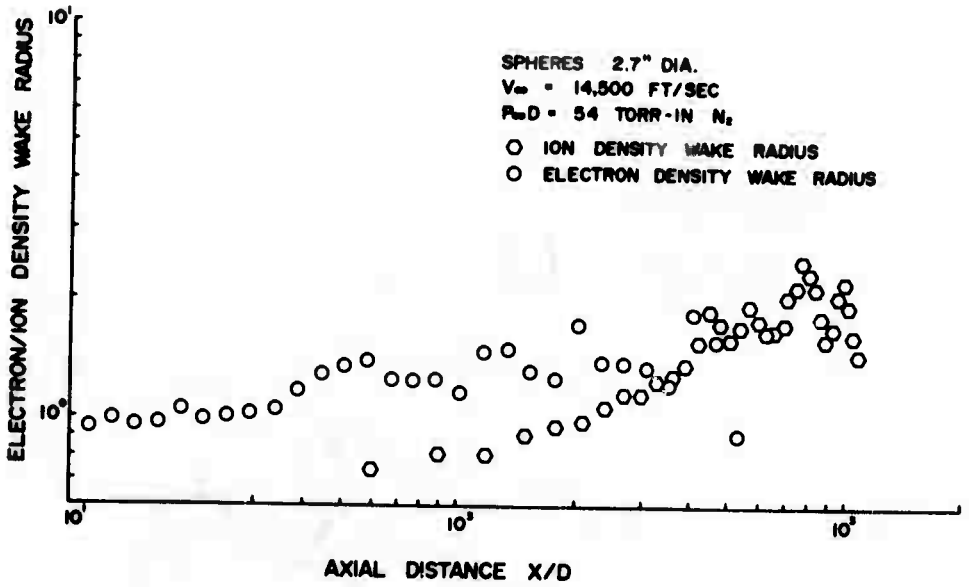

FIGURE 22

APPENDIX A

This appendix contains 12 tables which furnish all the numerical data concerning the fitting of gaussian profiles to the radial distributions of ion density estimates, both at 7.6 torr (20 torr-inches) and at 20 torr (54 torr-inches). Each table is associated with one particular theory and one given pressure. One finds tabulated in each table the same quantities, from left to right: the axial distance of the profile (X/D), the estimate of the ion density on the wake axis (n_o), the estimate of the wake ion density radius (r_i/D), the residual sum of the squares of the fit (R.S.S.), the standard deviation of the fit (S.D.), and finally, the number of individual measurements which form the radial profile (N). The ion density on the axis n_o is expressed in cm^{-3} and is normalized by 10^{10}. A value of r_i/D equal to 1000 signifies that the gaussian form of the profile has degenerated into a horizontal line. In that case the value of n_o is equivalent to the arithmetic mean of the measurements.

TABLE A-I

DATA RELATING TO FITS AT 7.6 TORR

Theory of Zakharova et al.

X/D	n_o	r_i/D	R.S.S.	S.D.	N
60.0	159.791	.94	.71248E+04	.12583E+02	47
90.0	108.765	1.04	.62675E+04	.10979E+02	54
120.0	66.769	1.25	.10127E+05	.13448E+02	58
150.0	45.437	1.41	.84163E+04	.12601E+02	55
180.0	31.234	1.62	.52989E+04	.98155E+01	57
210.0	23.674	1.98	.35919E+04	.75508E+01	65
240.0	19.522	2.03	.26219E+04	.62557E+01	69
270.0	12.450	4.35	.23614E+04	.62735E+01	62
300.0	9.434	1000.00	.16209E+04	.51548E+01	63
330.0	10.989	2.19	.12042E+04	.40615E+01	75
360.0	8.292	2.77	.81777E+03	.35470E+01	67
390.0	6.329	3.50	.55379E+03	.28967E+01	69
420.0	5.048	11.53	.87325E+03	.33039E+01	83
450.0	5.007	1000.00	.86932E+03	.32964E+01	82
480.0	4.577	1000.00	.52735E+03	.28267E+01	68
510.0	4.739	1000.00	.86638E+03	.39333E+01	58
540.0	5.344	1000.00	.97857E+03	.46123E+01	48
570.0	4.693	1000.00	.58773E+03	.39328E+01	40
600.0	5.085	3.53	.69216E+03	.43252E+01	39
630.0	4.773	3.76	.63949E+03	.43369E+01	36
660.0	5.470	2.33	.26407E+03	.31273E+01	29
690.0	8.517	1.96	.21992E+03	.34954E+01	20
720.0	6.244	3.46	.31402E+03	.39624E+01	22
750.0	3.900	1000.00	.25221E+03	.33115E+01	25
780.0	3.676	6.38	.10754E+03	.23790E+01	21
810.0	5.355	2.72	.68979E+02	.23035E+01	15
840.0	4.520	2.70	.54161E+02	.23273E+01	12
870.0	3.071	3.31	.29583E+02	.19230E+01	10
900.0	2.812	2.62	.50827E+01	.11272E+01	6

TABLE A-II

DATA RELATING TO FITS AT 7.6 TORR

Theory of Su and Kiel

X/D	n_o	r_i/D	R.S.S.	S.D.	N
60.0	35.857	1.00	.38157E+03	.29119E+01	47
90.0	25.257	1.11	.35424E+03	.26100E+01	54
120.0	16.322	1.36	.61137E+03	.33041E+01	58
150.0	11.639	1.57	.53477E+03	.31765E+01	55
180.0	8.365	1.90	.35206E+03	.25300E+01	57
210.0	6.611	2.51	.24609E+03	.19764E+01	65
240.0	5.708	2.59	.20054E+03	.17301E+01	69
270.0	4.022	1000.00	.19492E+03	.18024E+01	62
300.0	3.538	1000.00	.14790E+03	.15571E+01	63
330.0	3.583	3.20	.11837E+03	.12734E+01	75
360.0	2.866	6.02	.83650E+02	.11344E+01	67
390.0	2.393	17.24	.67298E+02	.10022E+01	69
420.0	2.299	1000.00	.10697E+03	.11492E+01	83
450.0	2.368	1000.00	.11272E+03	.11870E+01	82
480.0	2.233	1000.00	.71241E+02	.10389E+01	68
510.0	2.280	1000.00	.96667E+02	.13138E+01	58
540.0	2.524	1000.00	.10941E+03	.15423E+01	48
570.0	2.335	1000.00	.66187E+02	.13198E+01	40
600.0	2.138	1000.00	.70904E+02	.13843E+01	39
630.0	2.089	1000.00	.65043E+02	.13831E+01	36
660.0	2.227	4.37	.29603E+02	.10471E+01	29
690.0	2.790	3.80	.26175E+02	.12059E+01	20
720.0	2.580	11.95	.36718E+02	.13550E+01	22
750.0	2.148	1000.00	.32366E+02	.11863E+01	25
780.0	2.017	1000.00	.15541E+02	.90442E+00	21
810.0	2.375	5.24	.95793E+01	.85841E+00	15
840.0	2.149	4.87	.80733E+01	.89851E+00	12
870.0	1.692	8.99	.50821E+01	.79703E+00	10
900.0	1.597	5.57	.92359E+00	.48052E+00	6

TABLE A-III

DATA RELATING TO FITS AT 7.6 TORR

Theory of Schulz and Brown

X/D	n_o	r_i/D	R.S.S.	S.D.	N
60.0	30.388	.93	.25469E+03	.23790E+01	47
90.0	20.370	1.03	.21677E+03	.20417E+01	54
120.0	12.292	1.24	.34392E+03	.24782E+01	58
150.0	8.185	1.41	.27812E+03	.22907E+01	55
180.0	5.583	1.64	.17215E+03	.17692E+01	57
210.0	4.219	2.02	.11512E+03	.13518E+01	65
240.0	3.450	2.10	.81876E+02	.11055E+01	69
270.0	2.222	4.83	.72915E+02	.11024E+01	62
300.0	1.727	1000.00	.49465E+02	.90050E+00	63
330.0	1.928	2.38	.36608E+02	.70815E+00	75
360.0	1.468	3.21	.24923E+02	.61922E+00	67
390.0	1.130	4.38	.17784E+02	.51520E+00	69
420.0	.957	1000.00	.27445E+02	.58209E+00	83
450.0	.979	1000.00	.27226E+02	.58338E+00	82
480.0	.905	1000.00	.16539E+02	.50058E+00	68
510.0	.935	1000.00	.26519E+02	.68815E+00	58
540.0	1.047	1000.00	.30157E+02	.80968E+00	48
570.0	.940	1000.00	.17941E+02	.68713E+00	40
600.0	.949	4.74	.21071E+02	.75465E+00	39
630.0	.906	5.09	.19359E+02	.75457E+00	36
660.0	.995	2.88	.79719E+01	.54337E+00	29
690.0	1.403	2.43	.67591E+01	.61278E+00	20
720.0	1.159	4.41	.95001E+01	.68921E+00	22
750.0	.816	1000.00	.77202E+01	.57936E+00	25
780.0	.741	1000.00	.33312E+01	.41872E+00	21
810.0	1.004	3.43	.21117E+01	.40303E+00	15
840.0	.872	3.41	.16764E+01	.40944E+00	12
870.0	.633	4.75	.94667E+00	.34400E+00	10
900.0	.580	3.74	.16348E+00	.20217E+00	6

TABLE A-IV

DATA RELATING TO FITS AT 7.6 TORR

Theory of Kulgein

X/D	n_o	r_i/D	R.S.S.	S.D.	N
60.0	6.311	.87	.79724E+01	.42091E+00	47
90.0	4.041	.95	.61626E+01	.34425E+00	54
120.0	2.356	1.11	.87452E+01	.39518E+00	58
150.0	1.528	1.24	.62415E+01	.34317E+00	55
180.0	1.028	1.37	.38312E+01	.26393E+00	57
210.0	.779	1.55	.25331E+01	.20052E+00	65
240.0	.624	1.60	.16574E+01	.15728E+00	69
270.0	.410	2.13	.13540E+01	.15022E+00	62
300.0	.300	2.59	.83429E+00	.11695E+00	63
330.0	.347	1.71	.68135E+00	.96611E-01	75
360.0	.271	1.90	.47720E+00	.85683E-01	67
390.0	.199	2.21	.31672E+00	.68754E-01	69
420.0	.155	2.97	.43574E+00	.73345E-01	83
450.0	.128	6.65	.38165E+00	.69070E-01	82
480.0	.125	5.09	.24746E+00	.61233E-01	68
510.0	.143	3.65	.37445E+00	.81772E-01	58
540.0	.133	14.39	.38944E+00	.92012E-01	48
570.0	.151	3.24	.31815E+00	.91500E-01	40
600.0	.176	2.29	.45035E+00	.11032E+00	39
630.0	.157	2.63	.41157E+00	.11002E+00	36
660.0	.185	1.97	.18457E+00	.82680E-01	29
690.0	.348	1.50	.14268E+00	.89031E-01	20
720.0	.212	2.40	.19764E+00	.99408E-01	22
750.0	.137	3.42	.15698E+00	.82615E-01	25
780.0	.137	2.90	.78985E-01	.64476E-01	21
810.0	.187	2.23	.50087E-01	.62071E-01	15
840.0	.158	2.33	.37063E-01	.60880E-01	12
870.0	.116	2.65	.18626E-01	.48252E-01	10
900.0	.115	2.25	.33997E-02	.29154E-01	6

TABLE A-V

DATA RELATING TO FITS AT 7.6 TORR

Thin Sheath Theory of Clements and Smy

X/D	n_o	r_i/D	R.S.S.	S.D.	N
60.0	3.490	.86	.23965E+01	.23077E+00	47
90.0	2.203	.94	.18102E+01	.18658E+00	54
120.0	1.259	1.10	.25237E+01	.21229E+00	58
150.0	.799	1.22	.17517E+01	.18180E+00	55
180.0	.531	1.35	.10567E+01	.13861E+00	57
210.0	.399	1.52	.69041E+00	.10468E+00	65
240.0	.315	1.57	.43780E+00	.80835E-01	69
270.0	.204	2.08	.35065E+00	.76448E-01	62
300.0	.147	2.53	.20893E+00	.58525E-01	63
330.0	.170	1.68	.16750E+00	.47901E-01	75
360.0	.131	1.86	.11664E+00	.42360E-01	67
390.0	.095	2.16	.74965E-01	.33450E-01	69
420.0	.073	2.92	.10282E+00	.35628E-01	83
450.0	.060	6.49	.89990E-01	.33539E-01	82
480.0	.058	4.96	.57566E-01	.29533E-01	68
510.0	.067	3.63	.88716E-01	.39802E-01	58
540.0	.062	15.83	.93023E-01	.44969E-01	48
570.0	.071	3.16	.76228E-01	.44788E-01	40
600.0	.083	2.24	.10933E+00	.54359E-01	39
630.0	.074	2.59	.99474E-01	.54090E-01	36
660.0	.088	1.92	.43541E-01	.40158E-01	29
690.0	.175	1.44	.33378E-01	.43062E-01	20
720.0	.100	2.35	.46344E-01	.48137E-01	22
750.0	.063	3.36	.36232E-01	.39690E-01	25
780.0	.063	2.84	.17859E-01	.30659E-01	21
810.0	.087	2.20	.11301E-01	.29484E-01	15
840.0	.073	2.30	.82344E-02	.28696E-01	12
870.0	.053	2.62	.40370E-02	.22464E-01	10
900.0	.052	2.21	.73327E-03	.13540E-01	6

TABLE A-VI

DATA RELATING TO FITS AT 7.6 TORR

Thick Sheath Theory of Clements and Smy

X/D	n_o	r_i/D	R.S.S.	S.D.	N
60.0	1256.402	.80	.74932E+05	.59734E+02	23
90.0	1200.669	.86	.35086E+06	.11617E+03	28
120.0	1231.453	.87	.46625E+06	.12467E+03	32
150.0	960.817	.96	.63846E+06	.13506E+03	37
180.0	789.212	1.03	.63665E+06	.11764E+03	48
210.0	603.225	1.09	.31069E+06	.73189E+02	60
240.0	425.442	1.22	.33844E+06	.73295E+02	65
270.0	317.319	1.32	.30110E+06	.72681E+02	59
300.0	271.780	1.36	.19180E+06	.58523E+02	58
330.0	185.424	1.48	.74805E+05	.34188E+02	66
360.0	157.404	1.52	.90744E+05	.37080E+02	68
390.0	131.589	1.61	.11400E+06	.40356E+02	72
420.0	103.618	1.90	.10564E+06	.37283E+02	78
450.0	85.112	2.35	.87692E+05	.34899E+02	74
480.0	82.358	2.07	.56216E+05	.30112E+02	64
510.0	88.476	1.79	.36233E+05	.25903E+02	56
540.0	83.476	1.99	.42919E+05	.27684E+02	58
570.0	66.152	2.47	.42364E+05	.25931E+02	65
600.0	72.228	2.28	.81126E+05	.35328E+02	67
630.0	73.585	2.14	.83309E+05	.35800E+02	67
660.0	58.606	2.06	.41559E+05	.24906E+02	69
690.0	47.326	2.12	.19846E+05	.18340E+02	61
720.0	40.072	2.61	.15934E+05	.17178E+02	56
750.0	38.352	3.01	.18595E+05	.18731E+02	55
780.0	29.598	4.53	.15849E+05	.17629E+02	53
810.0	27.047	3.71	.13496E+05	.15958E+02	55
840.0	27.121	2.97	.11185E+05	.14956E+02	52
870.0	31.762	2.23	.72357E+04	.12972E+02	45
900.0	37.593	1.89	.57616E+04	.11575E+02	45
930.0	33.796	1.98	.66188E+04	.11743E+02	50
960.0	26.091	2.49	.64642E+04	.12406E+02	44
990.0	24.256	2.75	.74886E+04	.14227E+02	39
1020.0	24.441	2.52	.54426E+04	.12652E+02	36
1050.0	24.324	2.08	.23266E+04	.88064E+01	32
1080.0	25.740	1.82	.15278E+04	.87403E+01	22
1110.0	22.720	1000.00	.49100E+04	.17518E+02	18
1140.0	28.028	1000.00	.78730E+04	.19841E+02	22
1170.0	27.346	1000.00	.94660E+04	.21755E+02	22
1200.0	23.290	1000.00	.75559E+04	.19942E+02	21

TABLE A-VII

DATA RELATING TO FITS AT 20 TORR

Theory of Zakharova et al.

X/D	n_o	r_i/D	R.S.S.	S.D.	N
60.0	5.269	.88	.56139E+01	.35320E+00	47
90.0	3.437	.96	.45039E+01	.29430E+00	54
120.0	2.044	1.12	.65170E+01	.34114E+00	58
150.0	1.352	1.24	.47998E+01	.30094E+00	55
180.0	.917	1.38	.29933E+01	.23329E+00	57
210.0	.698	1.56	.19989E+01	.17813E+00	65
240.0	.563	1.60	.13350E+01	.14116E+00	69
270.0	.370	2.14	.11004E+01	.13542E+00	62
300.0	.273	2.59	.68725E+00	.10614E+00	63
330.0	.316	1.71	.56392E+00	.87892E-01	75
360.0	.246	1.89	.39528E+00	.77982E-01	67
390.0	.181	2.20	.26348E+00	.62709E-01	69
420.0	.141	2.95	.36247E+00	.66895E-01	83
450.0	.116	6.59	.31754E+00	.63002E-01	82
480.0	.113	5.03	.20618E+00	.55892E-01	68
510.0	.130	3.63	.31136E+00	.74565E-01	58
540.0	.120	13.88	.32367E+00	.83883E-01	48
570.0	.136	3.22	.26409E+00	.83365E-01	40
600.0	.159	2.28	.37303E+00	.10041E+00	39
630.0	.142	2.62	.34147E+00	.10022E+00	36
660.0	.168	1.95	.15378E+00	.75469E-01	29
690.0	.320	1.48	.11866E+00	.81192E-01	20
720.0	.192	2.39	.16461E+00	.90723E-01	22
750.0	.123	3.40	.13076E+00	.73399E-01	25
780.0	.124	2.88	.65791E-01	.58813E-01	21
810.0	.170	2.22	.41683E-01	.56625E-01	15
840.0	.143	2.32	.30773E-01	.55474E-01	12
870.0	.104	2.63	.15402E-01	.43877E-01	10
900.0	.104	2.23	.28098E-02	.26504E-01	6

TABLE A-VIII

DATA RELATING TO FITS AT 20 TORR

Theory of Su and Kiel

X/D	n_o	r_i/D	R.S.S.	S.D.	N
60.0	242.803	.84	.31988E+04	.12342E+02	23
90.0	235.117	.90	.14334E+05	.23480E+02	28
120.0	240.147	.91	.19263E+05	.25340E+02	32
150.0	192.652	1.01	.27011E+05	.27781E+02	37
180.0	159.482	1.09	.27521E+05	.24460E+02	48
210.0	121.153	1.18	.15111E+05	.16141E+02	60
240.0	87.193	1.34	.16568E+05	.16217E+02	65
270.0	66.933	1.48	.15036E+05	.16241E+02	59
300.0	58.204	1.55	.97129E+04	.13170E+02	58
330.0	41.147	1.74	.43108E+04	.82072E+01	66
360.0	35.413	1.81	.52292E+04	.89011E+01	68
390.0	31.067	1.90	.67422E+04	.98141E+01	72
420.0	25.767	2.27	.65005E+04	.92484E+01	78
450.0	22.397	2.86	.55039E+04	.87432E+01	74
480.0	21.971	2.45	.35553E+04	.75725E+01	64
510.0	23.743	2.05	.23067E+04	.65358E+01	56
540.0	22.854	2.27	.27773E+04	.70423E+01	58
570.0	18.535	3.06	.27704E+04	.66313E+01	65
600.0	19.491	2.90	.48787E+04	.86635E+01	67
630.0	19.609	2.72	.51772E+04	.89246E+01	67
660.0	16.561	2.54	.29729E+04	.66612E+01	69
690.0	14.100	2.65	.15121E+04	.50626E+01	61
720.0	12.523	3.39	.12416E+04	.47950E+01	56
750.0	12.054	4.22	.14302E+04	.51947E+01	55
780.0	9.760	18.36	.12653E+04	.49809E+01	53
810.0	9.057	7.51	.11233E+04	.46037E+01	55
840.0	9.162	4.40	.97500E+03	.44159E+01	52
870.0	10.430	2.90	.65861E+03	.39136E+01	45
900.0	11.843	2.40	.52791E+03	.35039E+01	45
930.0	11.004	2.51	.62226E+03	.36005E+01	50
960.0	9.214	3.21	.60550E+03	.37969E+01	44
990.0	8.719	3.64	.67106E+03	.42587E+01	39
1020.0	8.570	3.56	.50044E+03	.38365E+01	36
1050.0	8.410	2.92	.23357E+03	.27903E+01	32
1080.0	8.552	2.56	.15508E+03	.27846E+01	22
1110.0	8.845	1000.00	.47521E+03	.54499E+01	18
1140.0	10.514	1000.00	.73854E+03	.60768E+01	22
1170.0	10.397	1000.00	.86336E+03	.65702E+01	22
1200.0	9.204	1000.00	.72320E+03	.61695E+01	21

TABLE A-IX

DATA RELATING TO FITS AT 20 TORR

Theory of Schulz and Brown

X/D	n_o	r_i/D	R.S.S.	S.D.	N
60.0	292.756	.78	.37670E+04	.13393E+02	23
90.0	277.843	.85	.18522E+05	.26690E+02	28
120.0	285.172	.85	.24339E+05	.28483E+02	32
150.0	217.449	.93	.32727E+05	.30579E+02	37
180.0	176.834	1.01	.32191E+05	.26454E+02	48
210.0	134.331	1.06	.14436E+05	.15777E+02	60
240.0	92.998	1.19	.15733E+05	.15803E+02	65
270.0	68.401	1.29	.13807E+05	.15564E+02	59
300.0	58.007	1.34	.87564E+04	.12505E+02	58
330.0	38.450	1.47	.32058E+04	.70774E+01	66
360.0	32.273	1.51	.38825E+04	.76698E+01	68
390.0	26.645	1.62	.47677E+04	.82529E+01	72
420.0	20.856	1.90	.43336E+04	.75513E+01	78
450.0	17.085	2.37	.35539E+04	.70257E+01	74
480.0	16.445	2.10	.22696E+04	.60504E+01	64
510.0	17.572	1.81	.14577E+04	.51956E+01	56
540.0	16.584	2.02	.17217E+04	.55448E+01	58
570.0	13.147	2.52	.16958E+04	.51882E+01	65
600.0	14.447	2.31	.33420E+04	.71704E+01	67
630.0	14.732	2.17	.34035E+04	.72362E+01	67
660.0	11.616	2.11	.16297E+04	.49320E+01	69
690.0	9.353	2.20	.76847E+03	.36090E+01	61
720.0	7.962	2.73	.61265E+03	.33683E+01	56
750.0	7.642	3.17	.71592E+03	.36753E+01	55
780.0	5.923	5.15	.60594E+03	.34469E+01	53
810.0	5.417	4.15	.51397E+03	.31141E+01	55
840.0	5.430	3.23	.42487E+03	.29150E+01	52
870.0	6.284	2.39	.27400E+03	.25243E+01	45
900.0	7.368	2.00	.21835E+03	.22534E+01	45
930.0	6.665	2.10	.25081E+03	.22859E+01	50
960.0	5.245	2.67	.24511E+03	.24158E+01	44
990.0	4.917	2.97	.28422E+03	.27716E+01	39
1020.0	4.920	2.74	.20622E+03	.24628E+01	36
1050.0	4.817	2.30	.88259E+02	.17152E+01	32
1080.0	5.007	2.02	.58174E+02	.17055E+01	22
1110.0	4.725	1000.00	.18749E+03	.34232E+01	18
1140.0	5.769	1000.00	.30206E+03	.38863E+01	22
1170.0	5.652	1000.00	.36364E+03	.42641E+01	22
1200.0	4.861	1000.00	.29122E+03	.39150E+01	21

TABLE A-X

DATA RELATING TO FITS AT 20 TORR

Theory of Kulgein

X/D	n_o	r_i/D	R.S.S.	S.D.	N
60.0	23.498	.75	.20056E+02	.97726E+00	23
90.0	21.017	.82	.97459E+02	.19361E+01	28
120.0	21.140	.82	.12555E+03	.20457E+01	32
150.0	15.001	.91	.14622E+03	.20439E+01	37
180.0	11.917	.97	.13853E+03	.17354E+01	48
210.0	8.972	.99	.47837E+02	.90817E+00	60
240.0	5.963	1.10	.51260E+02	.90202E+00	65
270.0	4.271	1.17	.42048E+02	.85889E+00	59
300.0	3.603	1.19	.26394E+02	.68653E+00	58
330.0	2.286	1.29	.80224E+01	.35405E+00	66
360.0	1.905	1.31	.94525E+01	.37844E+00	68
390.0	1.509	1.41	.10689E+02	.39077E+00	72
420.0	1.159	1.60	.90956E+01	.34595E+00	78
450.0	.902	1.92	.73056E+01	.31854E+00	74
480.0	.851	1.78	.47643E+01	.27721E+00	64
510.0	.900	1.61	.29940E+01	.23547E+00	56
540.0	.848	1.75	.33989E+01	.24636E+00	58
570.0	.687	1.98	.33317E+01	.22997E+00	65
600.0	.783	1.83	.75157E+01	.34004E+00	67
630.0	.819	1.72	.76510E+01	.34309E+00	67
660.0	.632	1.70	.33087E+01	.22223E+00	69
690.0	.493	1.79	.15337E+01	.16123E+00	61
720.0	.410	2.09	.12090E+01	.14963E+00	56
750.0	.402	2.22	.13906E+01	.16198E+00	55
780.0	.317	2.60	.10874E+01	.14602E+00	53
810.0	.293	2.41	.95351E+00	.13413E+00	55
840.0	.291	2.23	.80238E+00	.12668E+00	52
870.0	.341	1.87	.51937E+00	.10990E+00	45
900.0	.411	1.65	.44725E+00	.10199E+00	45
930.0	.370	1.72	.51284E+00	.10336E+00	50
960.0	.280	2.09	.49970E+00	.10908E+00	44
990.0	.260	2.27	.61365E+00	.12878E+00	39
1020.0	.283	1.99	.45073E+00	.11514E+00	36
1050.0	.299	1.69	.19892E+00	.81429E-01	32
1080.0	.325	1.52	.13502E+00	.82164E-01	22
1110.0	.222	8.39	.32809E+00	.14320E+00	18
1140.0	.257	1000.00	.47514E+00	.15413E+00	22
1170.0	.247	1000.00	.52890E+00	.16262E+00	22
1200.0	.212	1000.00	.39842E+00	.14481E+00	21

TABLE A-XI

DATA RELATING TO FITS AT 20 TORR

Thin Sheath Theory of Clements and Smy

X/D	n_o	r_i/D	R.S.S.	S.D.	N
60.0	14.921	.78	.95206E+01	.67332E+00	23
90.0	13.612	.85	.41590E+02	.12648E+01	28
120.0	13.738	.85	.54989E+02	.13539E+01	32
150.0	10.244	.94	.67115E+02	.13848E+01	37
180.0	8.288	1.00	.64905E+02	.11878E+01	48
210.0	6.298	1.03	.26986E+02	.68211E+00	60
240.0	4.349	1.14	.28767E+02	.67573E+00	65
270.0	3.199	1.22	.24254E+02	.65231E+00	59
300.0	2.725	1.25	.15221E+02	.52135E+00	58
330.0	1.825	1.33	.52408E+01	.28616E+00	66
360.0	1.546	1.35	.61773E+01	.30593E+00	68
390.0	1.253	1.44	.72925E+01	.32277E+00	72
420.0	.977	1.63	.64056E+01	.29032E+00	78
450.0	.773	1.96	.52396E+01	.26976E+00	74
480.0	.735	1.81	.34298E+01	.23520E+00	64
510.0	.783	1.62	.21704E+01	.20048E+00	56
540.0	.740	1.76	.24760E+01	.21027E+00	58
570.0	.602	2.00	.24399E+01	.19680E+00	65
600.0	.676	1.86	.52754E+01	.28489E+00	67
630.0	.704	1.75	.54330E+01	.28911E+00	67
660.0	.554	1.73	.25030E+01	.19328E+00	69
690.0	.438	1.80	.11822E+01	.14155E+00	61
720.0	.366	2.11	.94066E+00	.13198E+00	56
750.0	.358	2.25	.10804E+01	.14277E+00	55
780.0	.285	2.61	.85793E+00	.12970E+00	53
810.0	.263	2.43	.75778E+00	.11957E+00	55
840.0	.261	2.24	.64101E+00	.11323E+00	52
870.0	.308	1.88	.41882E+00	.98691E-01	45
900.0	.370	1.65	.36069E+00	.91587E-01	45
930.0	.333	1.72	.41485E+00	.92967E-01	50
960.0	.253	2.09	.40361E+00	.98030E-01	44
990.0	.235	2.27	.49311E+00	.11544E+00	39
1020.0	.255	2.00	.36408E+00	.10348E+00	36
1050.0	.269	1.70	.16227E+00	.73546E-01	32
1080.0	.293	1.53	.11021E+00	.74234E-01	22
1110.0	.202	7.77	.26670E+00	.12911E+00	18
1140.0	.233	1000.00	.38334E+00	.13844E+00	22
1170.0	.223	1000.00	.42516E+00	.14580E+00	22
1200.0	.192	1000.00	.32206E+00	.13020E+00	21

TABLE A-XII

DATA RELATING TO FITS AT 20 TORR

Thick Sheath Theory of Clements and Smy

X/D	n_o	r_i/D	R.S.S.	S.D.	N
60.0	13.890	.74	.67340E+01	.56627E+00	23
90.0	12.315	.81	.32866E+02	.11243E+01	28
120.0	12.388	.81	.42265E+02	.11869E+01	32
150.0	8.718	.91	.49057E+02	.11839E+01	37
180.0	6.916	.96	.46337E+02	.10037E+01	48
210.0	5.243	.98	.15562E+02	.51799E+00	60
240.0	3.457	1.07	.16697E+02	.51481E+00	65
270.0	2.454	1.15	.13606E+02	.48856E+00	59
300.0	2.074	1.16	.85282E+01	.39024E+00	58
330.0	1.295	1.25	.24940E+01	.19740E+00	66
360.0	1.073	1.27	.29375E+01	.21097E+00	68
390.0	.837	1.37	.32607E+01	.21583E+00	72
420.0	.635	1.56	.27290E+01	.18949E+00	78
450.0	.486	1.88	.21714E+01	.17366E+00	74
480.0	.456	1.74	.14125E+01	.15094E+00	64
510.0	.480	1.58	.88472E+00	.12800E+00	56
540.0	.449	1.72	.10009E+01	.13369E+00	58
570.0	.363	1.94	.97668E+00	.12451E+00	65
600.0	.419	1.78	.22642E+01	.18664E+00	67
630.0	.440	1.68	.22862E+01	.18754E+00	67
660.0	.333	1.67	.94406E+00	.11870E+00	69
690.0	.256	1.75	.42984E+00	.85355E-01	61
720.0	.211	2.05	.33584E+00	.78862E-01	56
750.0	.207	2.17	.38700E+00	.85451E-01	55
780.0	.161	2.54	.29708E+00	.76322E-01	53
810.0	.149	2.35	.25774E+00	.69735E-01	55
840.0	.147	2.17	.21496E+00	.65568E-01	52
870.0	.173	1.83	.13717E+00	.56481E-01	45
900.0	.210	1.61	.11818E+00	.52425E-01	45
930.0	.187	1.69	.13469E+00	.52971E-01	50
960.0	.139	2.06	.13131E+00	.55915E-01	44
990.0	.130	2.24	.16278E+00	.66329E-01	39
1020.0	.142	1.95	.11863E+00	.59068E-01	36
1050.0	.151	1.64	.51251E-01	.41333E-01	32
1080.0	.166	1.47	.34670E-01	.41636E-01	22
1110.0	.109	10.00	.85280E-01	.73007E-01	18
1140.0	.128	1000.00	.12524E+00	.79132E-01	22
1170.0	.122	1000.00	.14050E+00	.83814E-01	22
1200.0	.105	1000.00	.10471E+00	.74238E-01	21

APPENDIX B

RADIAL DISTRIBUTIONS OF ION DENSITY, P_∞ = 7.6 TORR

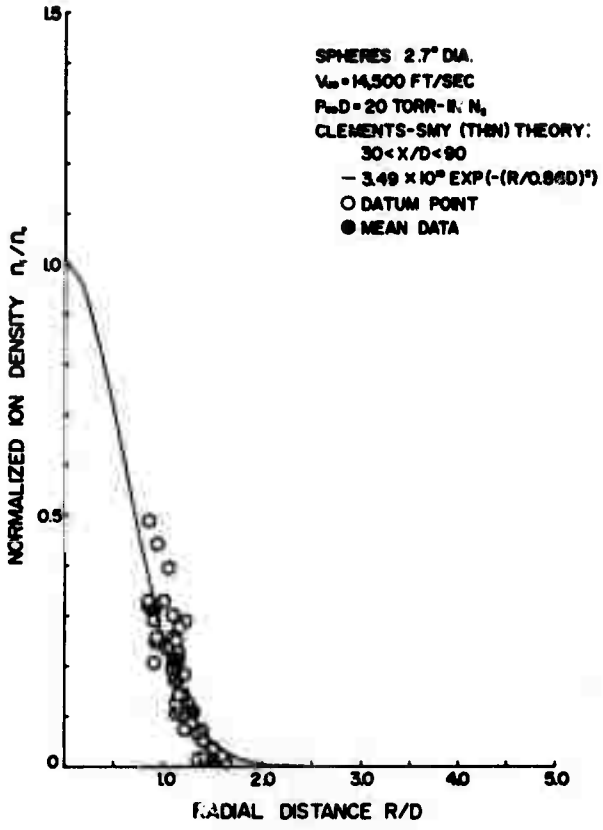

FIGURE B-1

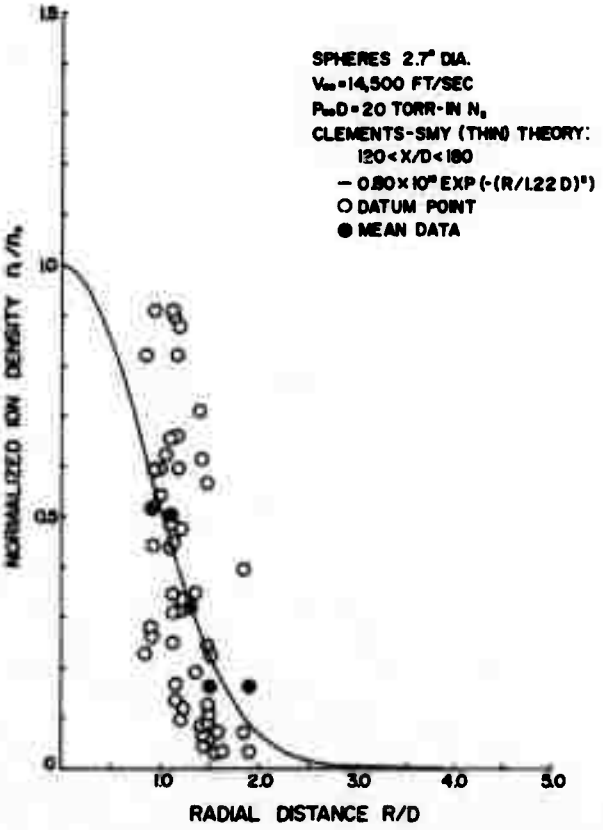

FIGURE B-2

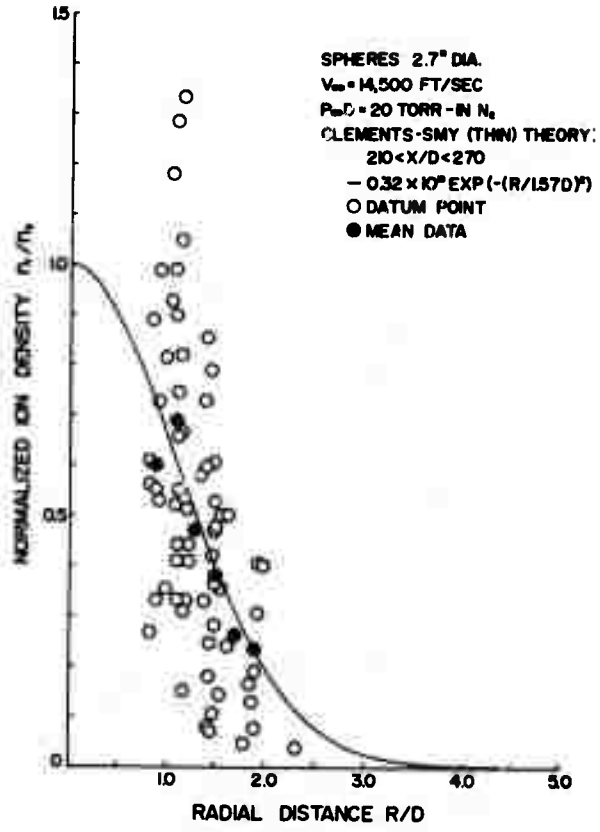

FIGURE B-3

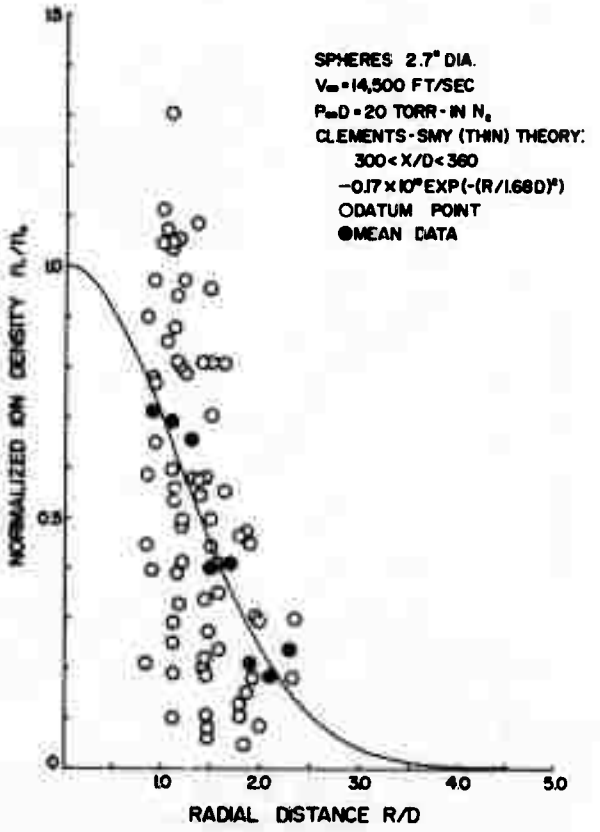

FIGURE B-4

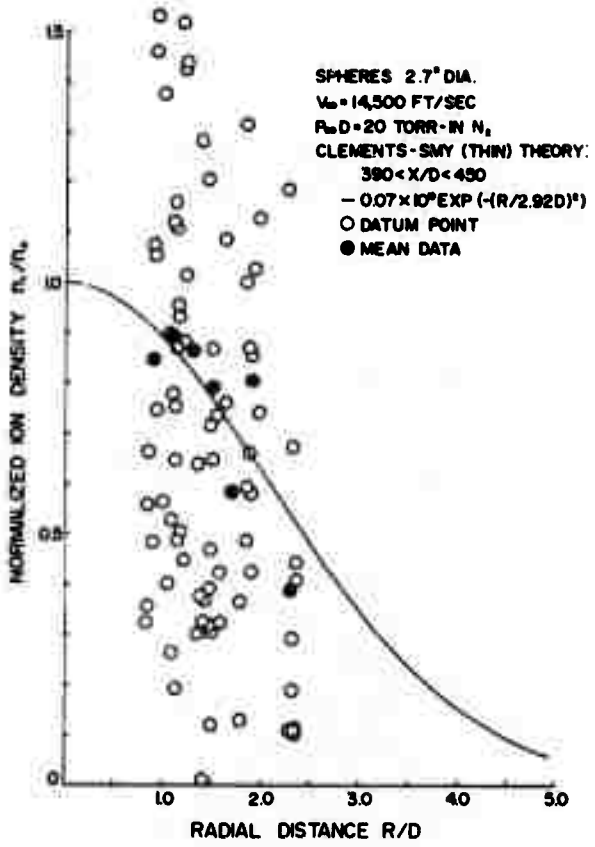

FIGURE B-5

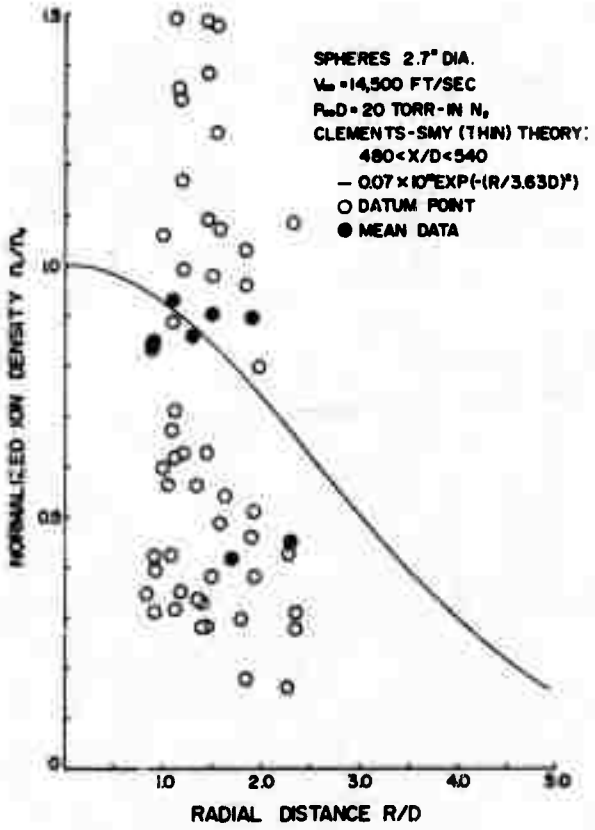

FIGURE B-6

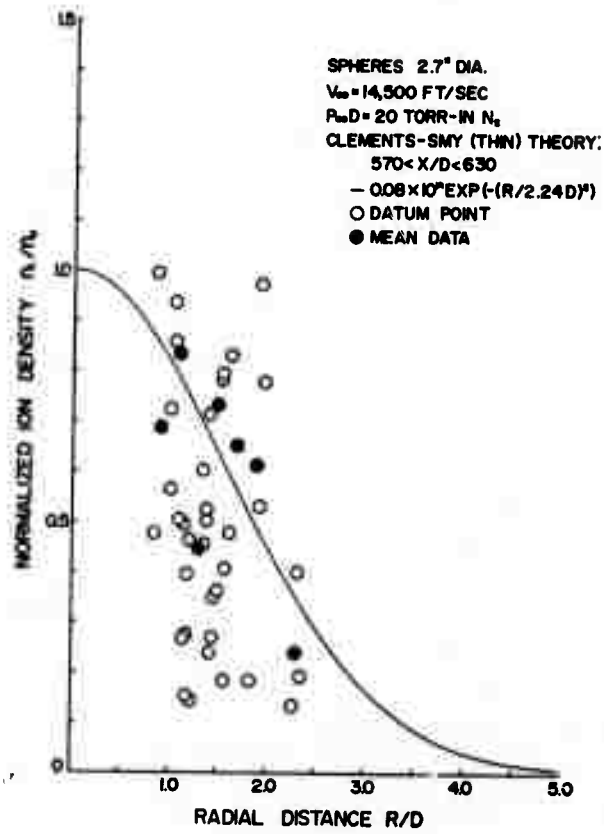

FIGURE B-7

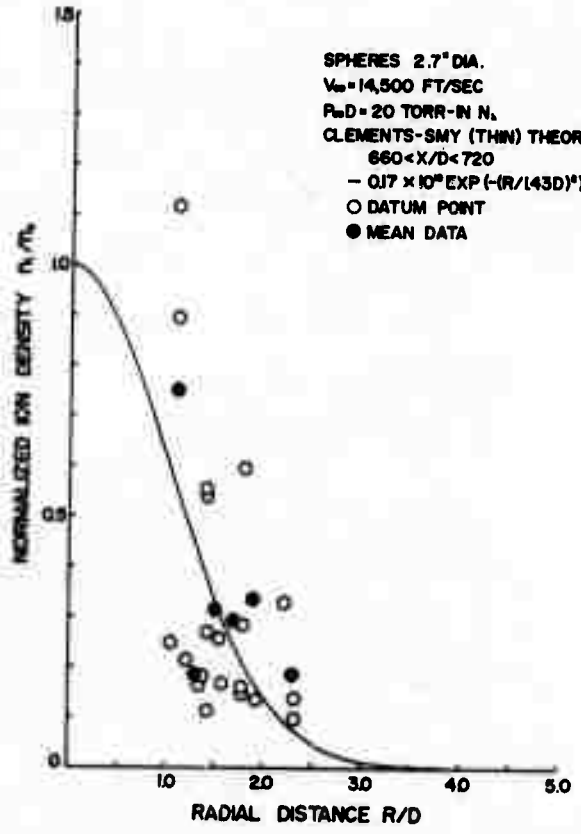

FIGURE B-8

APPENDIX C

RADIAL DISTRIBUTIONS OF ION DENSITY, P_∞ = 20 TORR

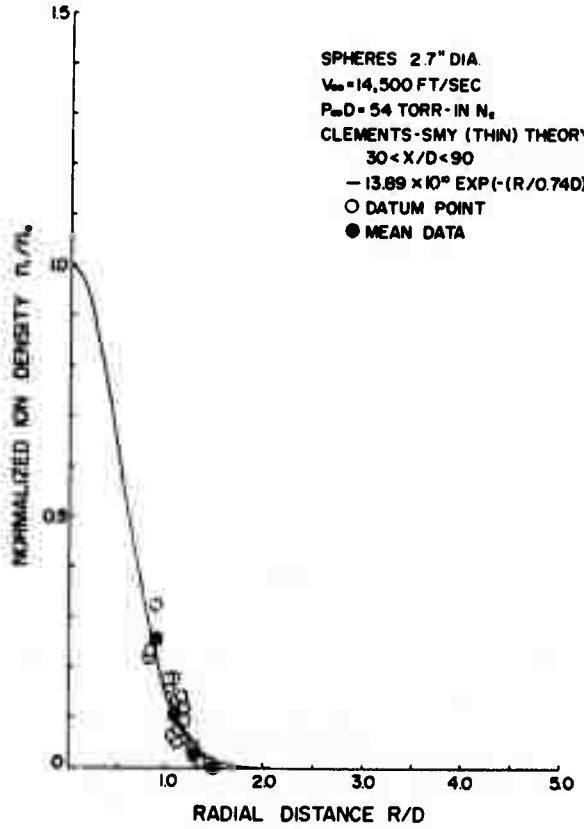

FIGURE C-1

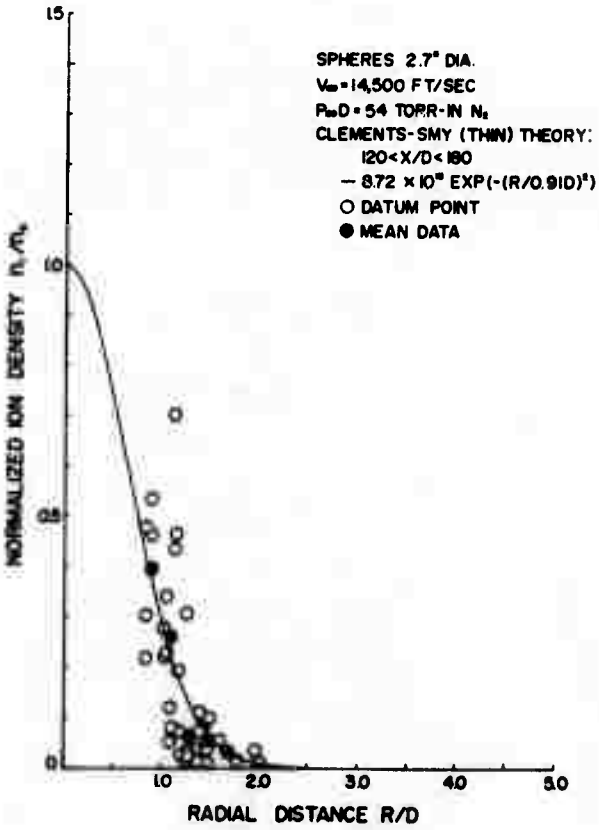

FIGURE C-2

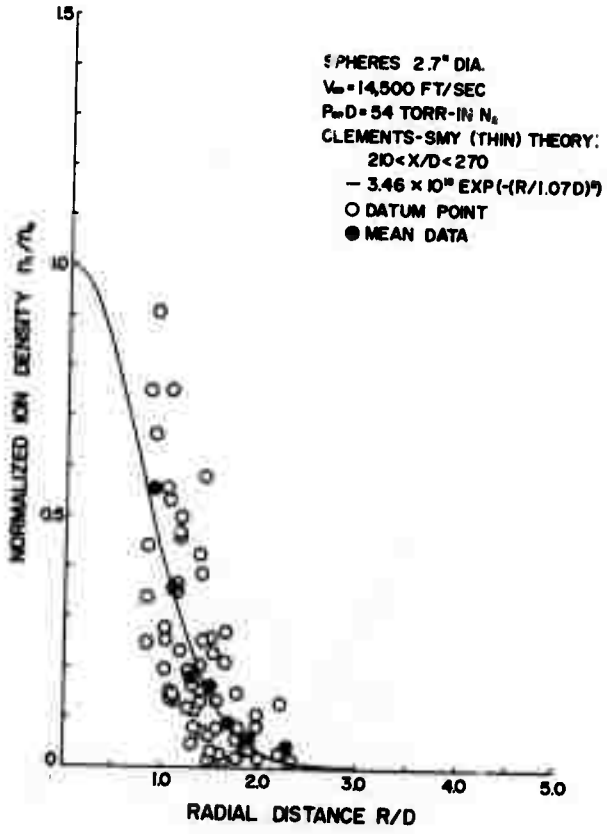

FIGURE C-3

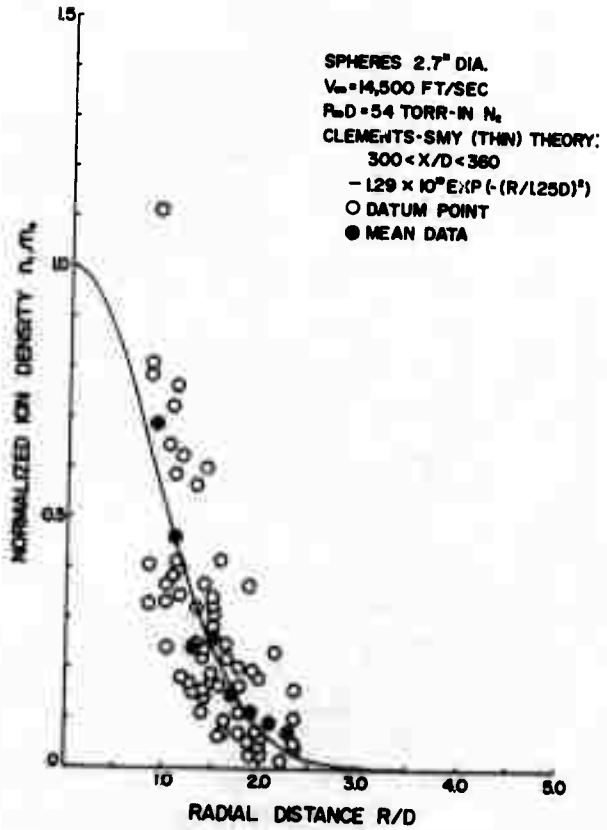

FIGURE C-4

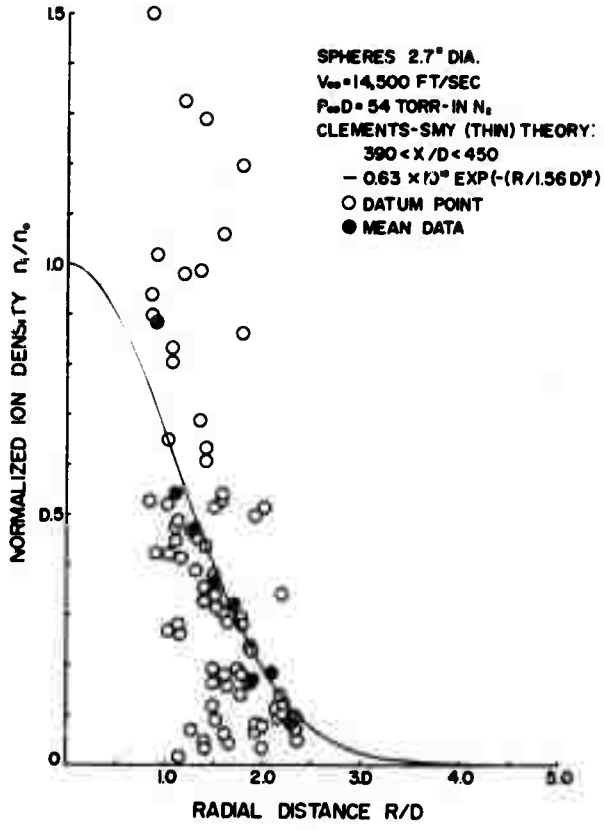

FIGURE C-5

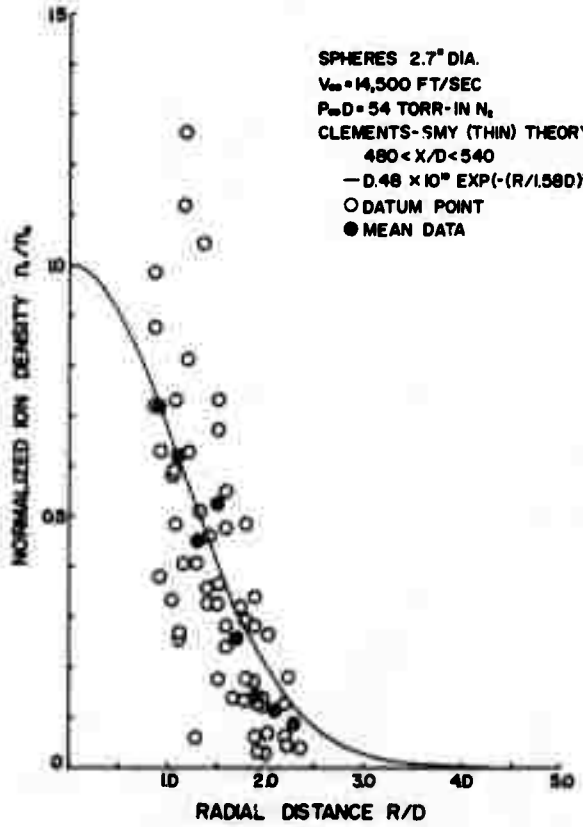

FIGURE C-6

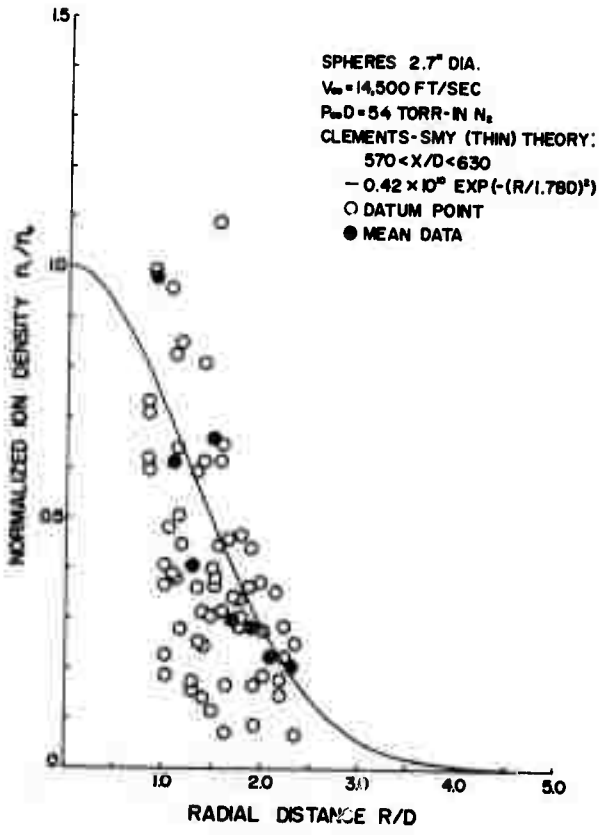

FIGURE C-7

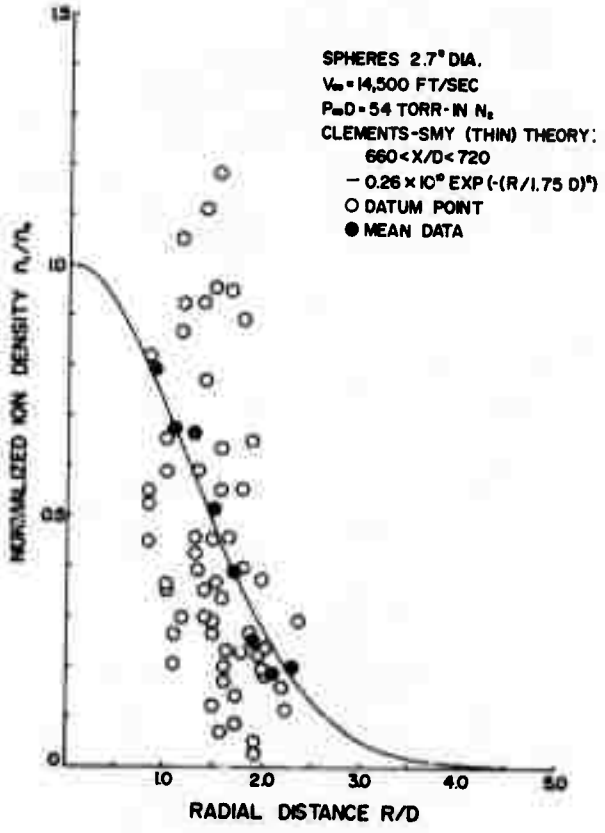

FIGURE C-8

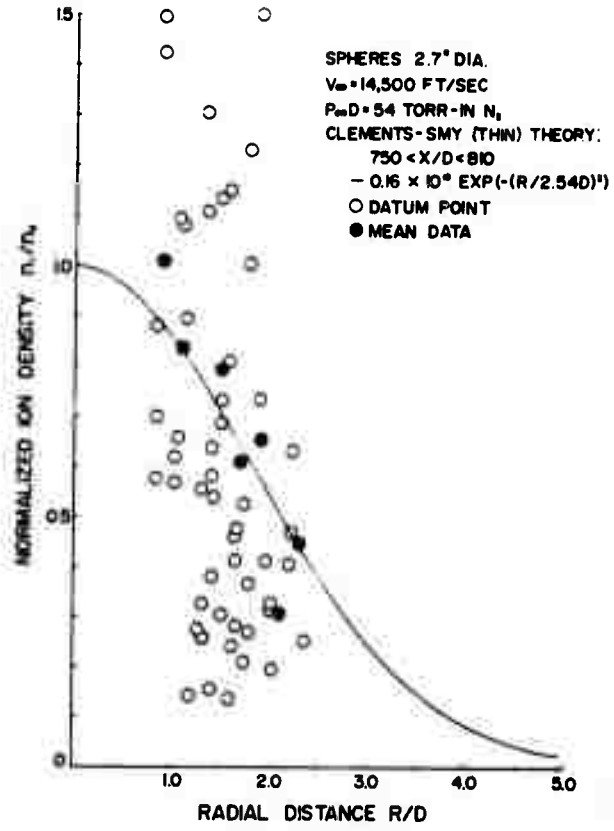

FIGURE C-9

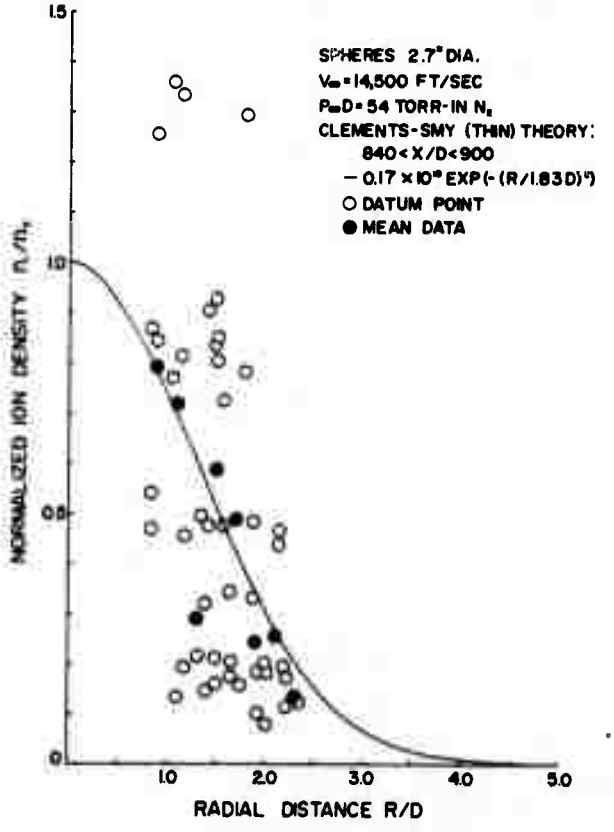

FIGURE C-10

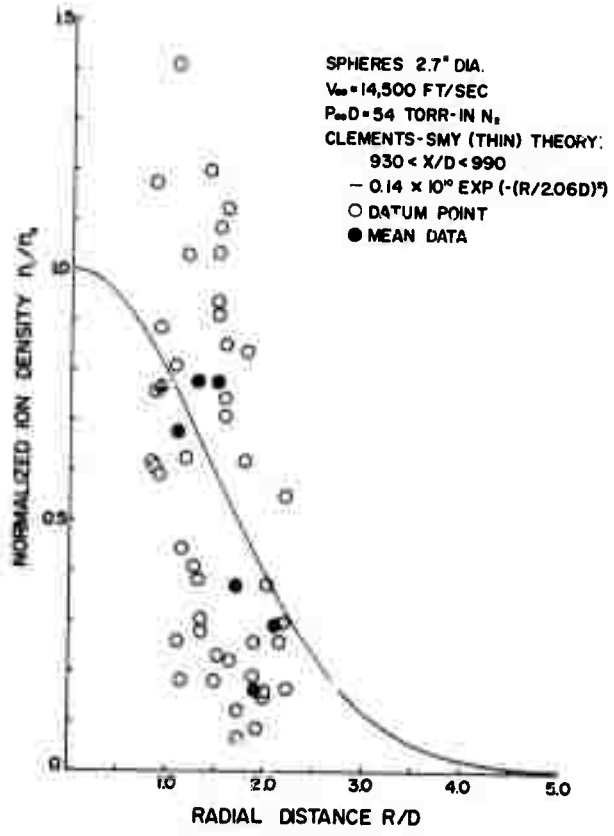

FIGURE C-11

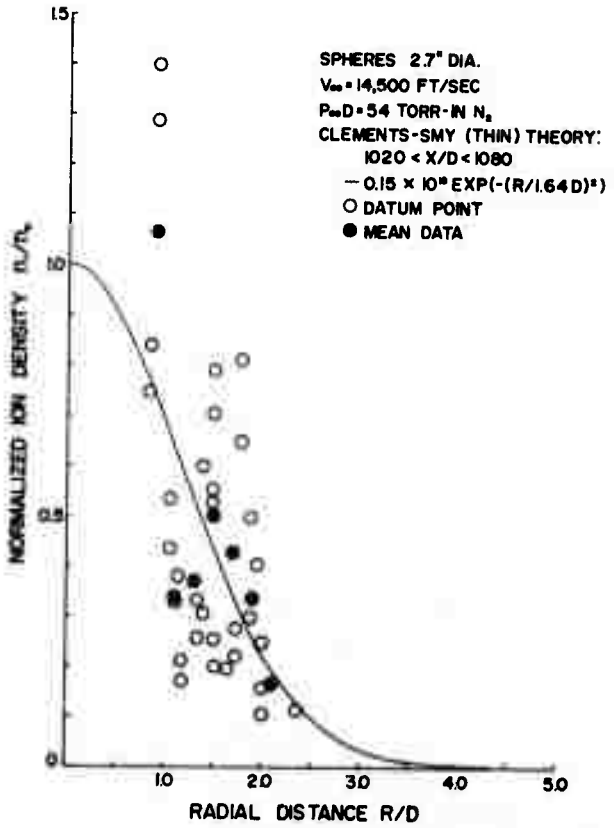

FIGURE C-12

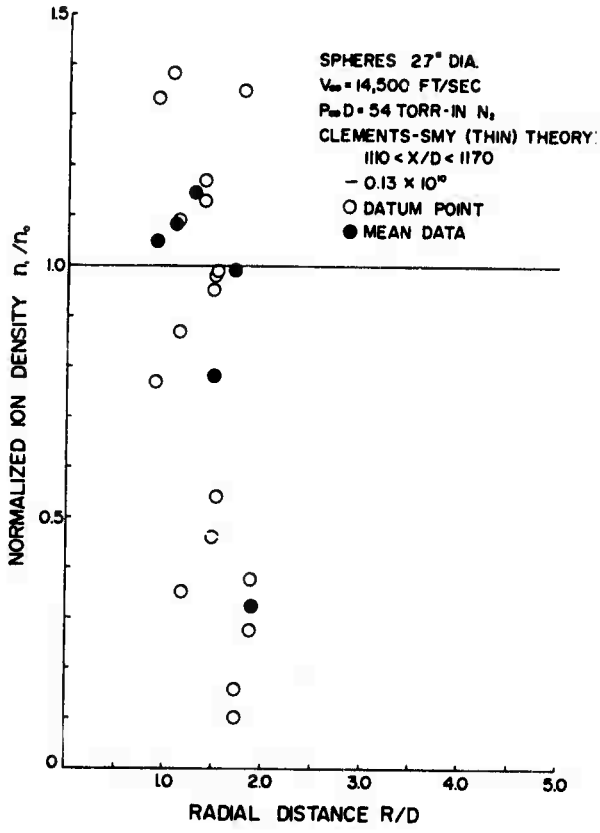
SPHERES 27" DIA.
V∞ = 14,500 FT/SEC
P∞D = 54 TORR-IN N2
CLEMENTS-SMY (THIN) THEORY:
1110 < X/D < 1170
– 0.13 x 10^10
O DATUM POINT
● MEAN DATA
NORMALIZED ION DENSITY n1/n0
1.5
1.0
0.5
0
1.0
2.0
3.0
4.0
5.0
RADIAL DISTANCE R/D

FIGURE C-13